THE EFFECT OF BI-AXIAL BEHAVIOUR OF MECHANICAL ANCHORS ON THE LATERAL RESPONSE OF MULTI-PANEL CLT SHEARWALLS

Authors: Mohammad Masroor[1]*, Ghasan Doudak[1], Daniele Casagrande[2]

Abstract

The importance of the bi-axial behaviour of some types of hold-downs and angle brackets has recently been identified, highlighting the need to include such effect in the analysis and design of Cross-Laminated Timber (CLT) shearwalls. The current study investigates elastic-plastic analytical methods for multi-panel CLT shearwalls, including the bi-axial contribution of the angle brackets and hold-downs connections and proposes expression in the elastic region to establish the Coupled-Panel (CP) and Single-Wall (SW) kinematic behaviours of the shearwall. The results from the elastic analysis show that considering the bi-axial effect of the angle brackets leads to more panels maintaining contact with the ground and resulting in less displacements and rotations. Sensitivity analyses are conducted to investigate the influence of the bi-axial contribution of the angle brackets. The proposed methodologies are verified using a numerical model, and the results showed that the analytical solution matches that obtained from the numerical model almost perfectly. Also, the methods are validated by comparing them with published experimental test results, and a reasonable match is obtained.

Keywords

Cross-laminated timber; Multi-panel Shearwalls; bi-axial behaviour; Analytical approach; Mechanical anchors; Lateral load.

---

[1] University of Ottawa, Department of Civil Engineering (Canada)

[2] Institute of Bioeconomy, National Research Council of Italy

*Corresponding Author, mmasr100@uottawa.ca

List of symbols

F concentrated lateral force applied on the top of the wall
F_j lateral horizontal load distributed in the j^{th} panel
$F_{c,y,j}$ internal force in each fastener in the vertical joints used for joining panel j to $j+1$
G equivalent shear deformation of CLT panels
K_{V,P_κ} lateral stiffness of the shearwall at point P_κ for $\kappa = [1{:}\,n_a + 2]$
R_{P_0} activation force
R_{P_κ} inelastic lateral capacity of the shearwall at point P_κ for $\kappa = [1{:}\,n_a + 2]$
$T_{a,x,i,j}$ horizontal force in the i^{th} angle bracket from the centre of rotation placed in panel j
$T_{a,z,i,j}$ uplift force in the i^{th} angle bracket from the centre of rotation placed in panel j
$T_{a,z,i}^{P_\kappa}$ uplift force in the i^{th} angle bracket at point P_κ for $\kappa = [1{:}\,n_a + 2]$
$T_{h,x}$ horizontal force in the hold-down
$T_{h,z}$ uplift force in the hold-down
$T_{h,z}^{P_\kappa}$ uplift force in the hold-down at point P_κ for $\kappa = [1, 2]$
W_{total} total potential energy in the system

b length of individual panel
$d_{y,ax}$ yielding displacement of the angle brackets in the horizontal direction (shear)
$d_{y,az}$ yielding displacement of the angle brackets in the vertical direction (uplift)
$d_{y,c}$ yield displacement of fasteners in the vertical joints
$d_{y,hx}$ yielding displacement of the hold-down in the vertical direction (uplift)
$d_{y,hz}$ yield displacement of the hold-down in the horizontal direction (shear)
$d_{u,ax}$ ultimate displacement of the angle brackets in the horizontal direction (shear)
$d_{u,az}$ ultimate displacement of the angle brackets in the vertical direction (uplift)
$d_{u,c}$ ultimate displacement of fasteners in the vertical joints
$d_{u,hx}$ ultimate displacement of the hold-down in the horizontal direction (shear)
$d_{u,hz}$ ultimate displacement of the hold-down in the vertical direction (uplift)
h height of the panels
k elastic stiffness of a fastener in the vertical joint
$\tilde{k}$ dimensionless stiffness ratio
$k_{a,x}$ elastic stiffness of an angle bracket in the horizontal direction (shear)
$k_{a,z}$ elastic stiffness of an angle bracket in the vertical direction (uplift)
$k_{h,x}$ elastic stiffness of a hold-down in the horizontal direction (shear)
$k_{h,z}$ elastic stiffness of a hold-down in the vertical direction (uplift)
k_v vertical contribution of hold-down and angle brackets in the total potential energy
k_v' contribution of the connections' stiffness in the rotation of panels
k_{v,P_κ}' contribution of the connections' stiffness in the uplift of panels at point P_κ for $\kappa = [1{:}\,n_a + 2]$
m number of panels in the shearwall
n number of fasteners per vertical joint
n_a number of angle brackets used in the length of each panel
q uniform vertical load applied on the top of the wall
$\tilde{q}$ dimensionless uniform vertical load
$r_{a,x}$ yield strength of angle brackets in the horizontal direction (shear)

$r_{a,z}$ yield strength of angle brackets in the vertical direction (uplift)
r_c yield strength of fasteners in the vertical joints
$r_{h,x}$ yield strength of hold-down in the horizontal direction (shear)
$r_{h,z}$ yield strength of hold-down in the vertical direction (uplift)
$t_{a,z,i}^{P_\kappa}$ increase in the uplift force of the i^{th} angle bracket from point $P_{\kappa-1}$ to P_κ for $\kappa = [1\!:n_a + 2]$
$t_{h,z}^{P_2}$ increase in the hold-down's uplift force at point P_2
v_j vertical displacement of panel j at the rotation point
$x_{\varphi=0}$ parameter studied when the vertical contribution of angle bracket is neglected
$x_{\varphi>0}$ parameter studied when the vertical contribution of angle bracket is considered

Δ_{P_0} lateral displacement due to sliding at the activation force (i.e., P_0)
Δ_{P_κ} lateral displacement at the top of the wall due to the rocking and sliding at point P_κ for $\kappa = [1\!:n_a + 2]$
Δ_r lateral displacement at the top of the wall due to the rocking
$\Delta_{r,s}$ lateral displacement at the top of the wall due to the rocking and sliding
Δ_s lateral displacement due to the sliding
Δ_{s,P_κ} lateral displacement due to the sliding at point P_κ for $\kappa = [3\!:n_a + 2]$
$\Delta_{sh,j}$ shear deformation in the j^{th} panel
Δ_{total} total lateral displacement due to the rocking, sliding and shear deformation
$\emptyset$ variable considering the effect of multiple angel brackets used in sensitivity analysis

α coefficient incorporating the effect of multiple angle brackets used in the length of panels
β coefficient incorporating the effect of compression zone in the panels
γ_a ratio incorporating the effect of multiple angle brackets in the limit expression of CP kinematic region
δ_{P_κ} increase in the total lateral displacement from point $P_{\kappa-1}$ to P_κ for $\kappa = [2\!:n_a + 2]$
φ angle bracket's vertical stiffness ratio
$\rho(x)$ ratio of the studied parameter x
ϑ angle of rotation of the panels

1. Introduction

Cross Laminated Timber (CLT) panels have increasingly been used in mid- and high-rise buildings in the past decade, especially in Europe and North America. The appeal of using this material has primarily been due to its structural reliability, environmental benefits and rapid construction process.

In high wind and seismic regions, CLT walls are typically relied upon to resist both gravity and lateral loads. The analysis and design procedures for gravity loads are clearly outlined in timber design standards (e.g., [1, 2]), however, methodologies to design CLT shearwalls to resist lateral loads still lacks development. Although some general provisions, mainly based on hierarchy of failure amongst various components in the wall assembly, have been enacted, no clearly defined design method currently exist. Consequently, simplistic analysis assumptions based on the static methods, or comprehensive modelling techniques involving sophisticated 3-D finite element models, have been used by designers.

Experimental investigations of the behaviour of CLT shearwalls subjected to lateral in-plane loading have revealed that the wall assembly exhibits rigid-body deformation in the CLT panels, due to their high in-plane rigidity, while the non-linearity is principally achieved in the connections [3, 4, 5]. This emphasizes the importance of the connection behaviour and their contribution to the strength, stiffness and ductility of the wall assembly and the building as a whole. Such connections typically consist of vertical joints that connect the individual CLT panels together, hold-downs, which are typically placed at the ends of the shearwall, and angle brackets with the capability to resist the shear force from the wall to the foundation or floor below.

Several full-scale experimental and numerical studies have been undertaken in order to investigate the seismic behaviour of CLT assemblies. Ceccotti et al. [3] conducted shake-table tests on a seven-storey CLT structure consisting of multi-panel shearwalls with high-strength hold-downs. The building was reported to perform well even after being subjected to several ground motions, and only local damage in the connectors was observed. Flatscher et al. [6] investigated the behaviour of connectors used in CLT walls by conducting an experimental campaign as part of the SERIES research project. A full-scale test was performed on a three-story CLT structure with single-panel shearwalls, and as a result, smaller drift values were observed when compared to the study involving multi-panel shearwalls [3]. Popovski and Gavric [7] investigated the seismic behaviour of a full-scale twostory CLT structure, constructed with multi-panel walls and comprised of hold-downs, angle brackets and vertical joints. The authors reported no overall instability in the structure, while more deformations were observed in the vertical joints connecting the individual shearwall panels. Yasumura et al [8] conducted experimental testing on two buildings with two storeys, constructed with single-panel and multi-panel CLT walls with openings. The results showed minor cracks in the corners of some openings within the single-panel walls, whereas no visible cracks were observed in the opening when multi-panel walls were used. Rinaldin and Fragiacomo [9] performed nonlinear simulations of the specimens reported in [3], based on a proposed finite element model. Reasonable match was observed when the experimental results were compared to the simulated models.

Due to the importance of the connection contribution in CLT wall assemblies, some studies have focussed on establishing the connection behaviour in isolation as well as part of the wall system. Of relevance to the current study is the investigation of the bi-axial behaviour (vertical uplift and horizontal shear) of some types of angle brackets. Shen et al. [10] performed experimental testing at the connection level for some angle brackets, as well as at the wall level. Numerical simulation was used to determine the hysteresis behaviour of angle brackets based on the results obtained from the experimental campaign. Gavric et al. [11] carried out tests on hold-down and angle bracket connectors. The authors reported stiffness values for the angle brackets that were of similar magnitude in the vertical and horizontal directions. Reported stiffness values for the hold-down in shear were less than those in uplift but they were not insignificant. Similarly, Flatscher et al. [6] and Schneider et al. [12] reported relatively high stiffness and capacity of angle bracket when subjected to uplift loads. Pozza et al. [13, 14] investigated the axial-shear interaction effect of angle brackets and proposed a numerical model to develop their hysteretic behaviour. Pozza et al. [15] also investigated the interaction of shear and axial behaviours in the hold-down connection. Liu and Lam [16, 17] and Liu et al. [18] also emphasized the need to include the coupled behaviour of angle brackets and hold-downs in the analysis since the interaction between the uplift and horizontal shear could have a significant effect on the wall behaviour. D'Arenzo et al. [19] proposed an innovative angle bracket for CLT wall-to-floor connection fastened with fully threaded screws that helped improve the tension behaviour of the angle brackets.

Analytical methods have also been developed in order to evaluate the design parameters of CLT shearwalls, including internal forces in connectors as well as rotation and lateral displacement of the wall [20]. Gavric et al. [21] proposed analytical methods for analyzing two-panel CLT shearwalls, using moment equilibrium, where the bi-axial effect of the hold-down and angle brackets were considered. Comparisons between the analytical approach and the experimental tests showed that the proposed analytical method may under- or over-estimate the shearwall behaviour for different practical cases. Flatscher and Schickhofer [22] established an iterative displacement-based method for single-panel and two-panel CLT shearwalls, where rotation, displacement and internal forces in connectors can be determined. Tamagnone et al. [23] developed a nonlinear design methodology for single-panel CLT shearwalls using sectional design method. Casagrande et al. [24] proposed an analytical approach in the elastic region for multi-panel CLT shearwalls using minimum potential energy, where expressions for the wall capacity, rotation, displacement and stiffness were developed. Nolet et al. [25] extended the study by Casagrande et al. [24] to include a more comprehensive method for multi-panel CLT shearwalls, while considering different possible failure mechanisms and assuming that the connectors have elastic-perfectly plastic behaviour.

The review of the available literature highlights the need to develop a comprehensive analytical method in which the bi-axial behaviour of angle brackets and hold-downs are considered for multi-panel CLT shearwalls. Such comprehensive approach is achieved in this study by building on existing models found in the literature [24, 25] and contributing to specific gaps in knowledge. Examples of contributions in the proposed model include considering the contribution of multiple angle brackets along the wall length, bi-axial contribution of both the hold-down and angle bracket connections, as well as accounting for the effect of compression zone in the CLT panel. The proposed model is verified using numerical models and validated against published experimental test results.

2. Development of analytical methods for multi-panel CLT shearwalls

2.1. Notations and assumptions

Figure 1 shows the investigated shearwalls and the placement of the connections used in this study. A hold-down is assumed at the ends of the shearwall, and equally spaced angle brackets connecting each wall panel to the floor below are assumed to be placed along the panel length. The shearwall consists of m panels that are connected to each other using vertical joints. The shearwalls are assumed to be subjected to a vertical uniformly distributed gravity load, q, and a concentrated lateral load, F.

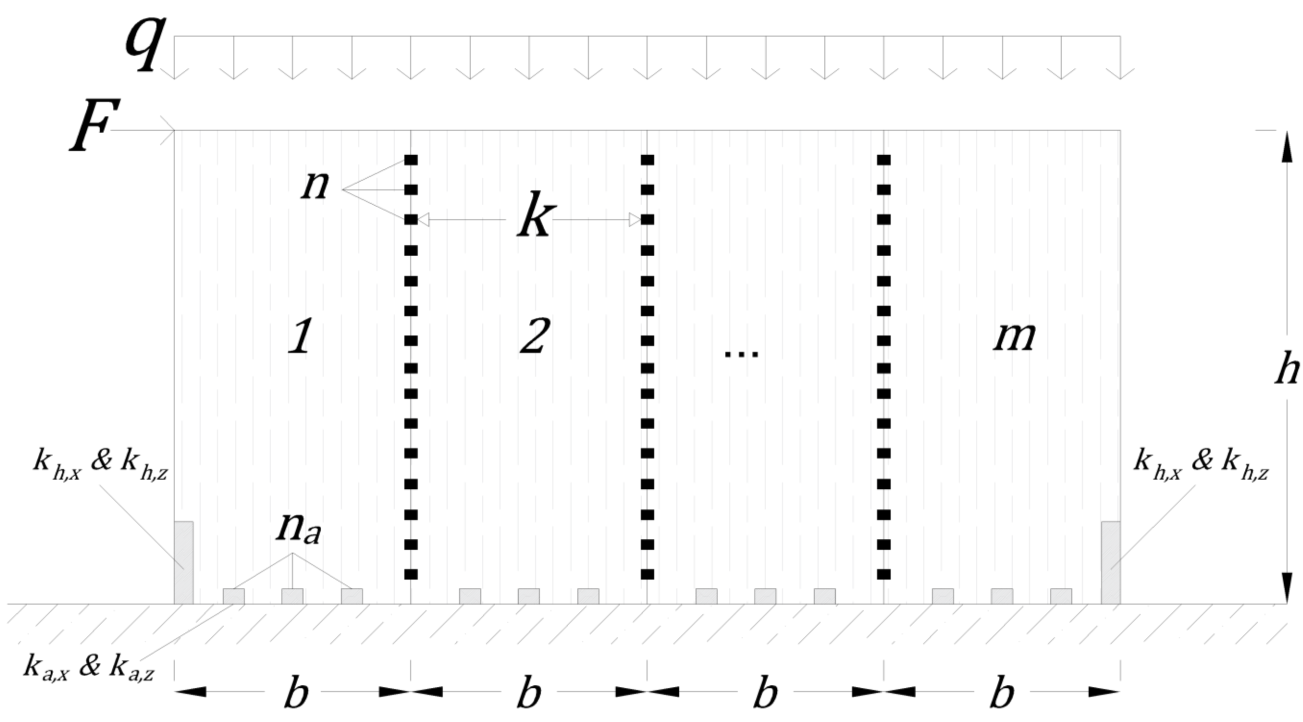

Figure 1: Multi-panel CLT shearwalls with typical connection and loading configuration

The hold-down connectors in this model are assumed to resist both vertical (uplift) and horizontal (shear) loads, n fasteners in each vertical joint are used to connect the panels together, and n_a equally spaced angle brackets, capable of resisting both uplift and shear, are considered. The stiffness of the hold-down in the vertical and horizontal directions and the stiffness of the vertical joints are denoted $k_{h,z}$, $k_{h,x}$ and k, respectively. The angle brackets are assigned horizontal and vertical stiffness of $k_{a,x}$ and $k_{a,z}$, respectively.

Based on the mechanical properties of connectors and the applied loads, three kinematic behaviours can be defined, as reported in [24]: 1) Coupled-wall (CP), where one center of rotation for each panel is attained, 2) Single-wall (SW), where only one global point of contact for the entire wall is attained, and 3) Intermediate behaviour (IN), which represents a special case, where only some panels are in contact with the ground.

The general assumptions used in the development of the proposed approach are:

- The same horizontal displacement is assumed for all points at the top and bottom of the shearwall due to the in-plane diaphragm behaviour of the floor elements.
- CLT panels are assumed as rigid elements for the purpose of investigating the kinematic behaviour.

The first assumption is attributed to the high in-plane stiffness in the diaphragm as well as the connection between the CLT floor and the shearwall. Regarding the second assumption, the contribution from the panel deformation has been found to be relatively small, and as such assuming the panels to be perfectly rigid is a reasonable approximation based on the results obtained from experimental tests (e.g., [3, 4, 5]). It should be noted that the contribution from the panel deformation may be significant for certain wall configurations, such as panels with very high aspect ratios, and walls with openings. In those cases, the flexure and shear deformation of the panels can be considered independently of the rocking and sliding deformations, and methods that account for such contribution are readily available in the literature (e.g., [21, 22]). Furthermore, experimental investigations of CLT shearwalls (e.g., [4, 6]) have shown that the centers of rotation of the wall segments may not be located at the corner of each panel due to the presence of a compressive zone in the panel. This effect is incorporated in the proposed model by assuming a reduced length of panel equal to $b \cdot \beta$ in the CP behaviour. Such contribution can be neglected by adopting β equal to unity.

In the following sections, the equations for CP and SW are developed, and the required analytical expressions are determined.

2.2 Elastic analytical procedure to achieve CP behaviour

The analytical variables in the CP case include the horizontal displacement due to panel sliding, denoted as Δ_s, and the angle of rotation of the panels, defined as ϑ, which is equal for all panels due to the diaphragm constraint (Figure 2). The connectors are defined as elastic springs, where the hold-downs are assumed to resist uplift and shear, vertical joints resist the shear force transferred between panels, and the angle brackets are considered as two springs along the bottom edge of the wall panels.

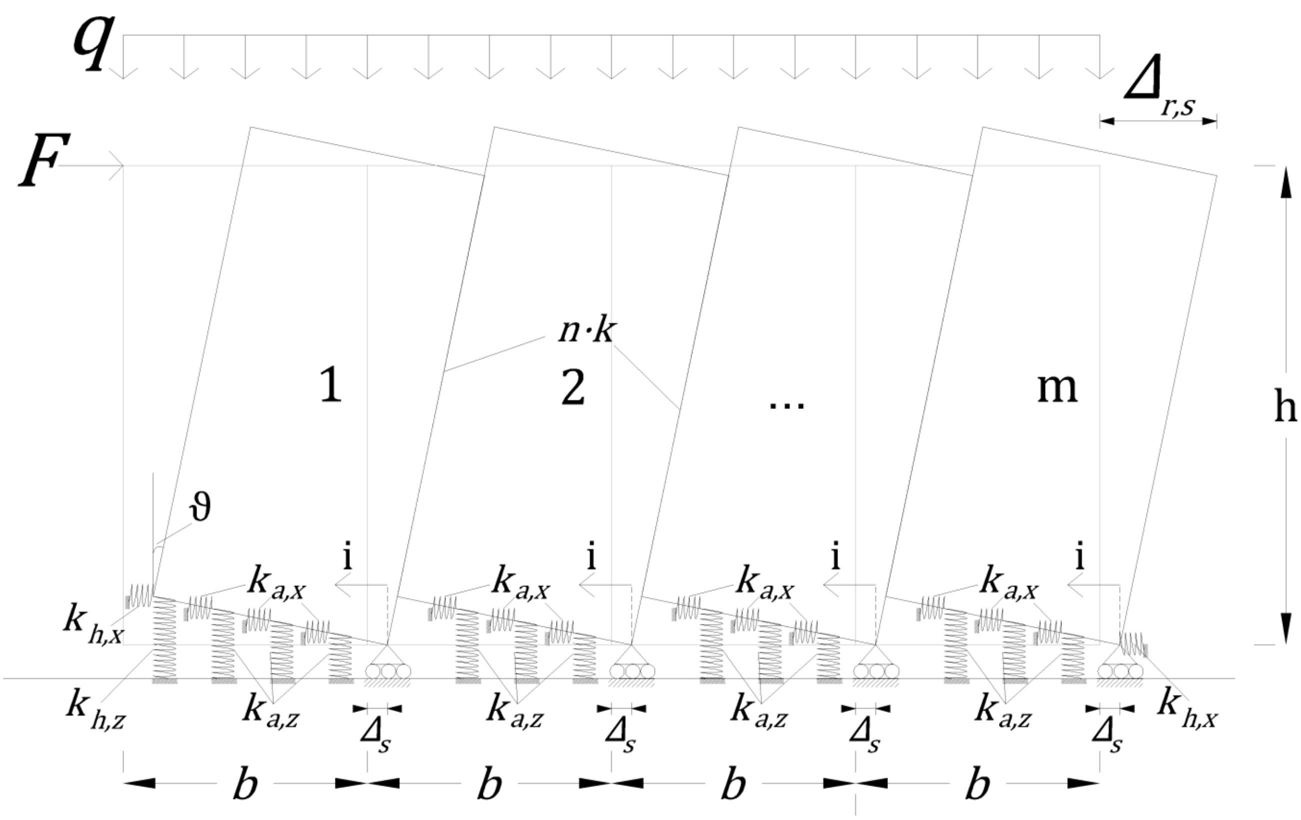

Figure 2: CLT multi-panel shear wall CP behaviour

The relationship between the vertical stiffness of the hold-down and the angle brackets is presented in Equation (1), where φ represents the angle brackets' vertical stiffness ratio. This equation expresses a measure for the contribution of the angle brackets in the vertical direction and facilitates the comparison between including and excluding such contribution.

$$k_{a,z} = \varphi \cdot k_{h,z} \tag{1}$$

The total contribution of the hold-down and angle brackets to the vertical stiffness k_v can be defined as shown in Equation (2), obtained using the total potential energy. Equation (2) contains the flexibility of including multiple angle brackets by introducing the coefficient α, as expressed in Equation (3).

$$k_v = k_{h,z} \cdot (\beta^2 + \alpha \cdot \varphi \cdot m) \tag{2}$$

$$\alpha = \sum_{i=1}^{n_a} \left[\frac{i}{(n_a + 1)} + (\beta - 1)\right]^2 \tag{3}$$

Based on the model proposed in Figure 2, the total potential energy in CP behaviour is developed, as shown in Equation (4). It should be noted that this equation includes the angle brackets' vertical stiffness (incorporated in k_v) and the sliding effect of the angle brackets and hold-downs, which are independent from the rocking motion. The contribution of the connectors' stiffness in rotation is denoted k_v', and obtained using Equation (5), which combines the stiffness effect in the vertical direction of the hold-down and the angle brackets as well as the effect of the vertical joints.

$$\begin{aligned} W_{total} &= \frac{1}{2} \cdot b^2 \cdot \vartheta^2 \cdot k_v' + \left(\frac{1}{2} k_{a,x} \cdot n_a \cdot m + k_{h,x}\right) \cdot {\Delta_s}^2 - F \cdot (h \cdot \vartheta + \Delta_s) \\ &+ \frac{q \cdot m \cdot b^2 \cdot (2 \cdot \beta - 1)}{2} \cdot \vartheta \end{aligned} \tag{4}$$

$$k_v' = k_v + (m - 1) \cdot n \cdot k \cdot \beta^2 \tag{5}$$

By equating the first derivative of the total potential energy, defined in Equation (4), to zero, the angle of rotation, ϑ, and the lateral displacement due to sliding, Δ_s, can be recovered, as shown in Equations (6) and (7). It can be noted from Equation (7) that the sliding of the wall only depends on the horizontal stiffness of the angle brackets and hold-downs.

$$\vartheta = \left[\frac{F \cdot h}{b^2} - \frac{q \cdot m \cdot (2 \cdot \beta - 1)}{2}\right] \cdot \frac{1}{k_v'} \tag{6}$$

$$\Delta_s = \frac{F}{k_{a,x} \cdot m \cdot n_a + 2 \cdot k_{h,x}} \tag{7}$$

The lateral displacement at the top of the wall, $\Delta_{r,s}$, is defined in Equation (8), by considering both rocking (Δ_r) and sliding (Δ_s) effects:

$$\Delta_{r,s} = \Delta_r + \Delta_s = \vartheta \cdot h + \Delta_s \tag{8}$$

The internal forces in the connectors can be obtained by multiplying the displacement with the stiffness of the associated connectors. The internal forces in the vertical joints, $F_{c,y,j}$, can be obtained using Equation (9) for panel j. The internal forces in all fasteners used in the vertical joints are equal due to equal displacements in the joints, when the CP behaviour is achieved.

$$F_{c,y,j} = \left[\frac{F \cdot h}{b^2} - \frac{q \cdot m \cdot (2 \cdot \beta - 1)}{2}\right] \cdot \frac{k \cdot b \cdot \beta}{k'_v}, \qquad j = [1\colon m-1] \tag{9}$$

The uplift forces in the hold-down and the i^{th} angle bracket away from the center of rotation of each panel (see Figure 2), can be expressed as presented in Equation (10) and (11), respectively. These equations are derived by multiplying the associated displacement with the stiffness of the connector.

$$T_{h,z} = \left[\frac{F \cdot h}{b^2} - \frac{q \cdot m \cdot (2 \cdot \beta - 1)}{2}\right] \cdot \frac{k_{h,z} \cdot b \cdot \beta}{k'_v} \tag{10}$$

$$T_{a,z,i,j} = \left[\frac{i}{n_a + 1} + (\beta - 1)\right] \cdot \left[\frac{F \cdot h}{b^2} - \frac{q \cdot m \cdot (2 \cdot \beta - 1)}{2}\right] \cdot \frac{\varphi \cdot k_{h,z} \cdot b}{k'_v}, \quad j = [1\colon m], i = [1\colon n_a] \tag{11}$$

The horizontal forces in each angle bracket and hold-down can be calculated using Equations (12) and (13), respectively.

$$T_{a,x,i,j} = \frac{F \cdot k_{a,x}}{k_{a,x} \cdot m \cdot n_a + 2 \cdot k_{h,x}}\ , \qquad j = [1{:}\,m]\ \&\ i = [1{:}\,n_a] \tag{12}$$

$$T_{h,x} = \frac{F \cdot k_{h,x}}{k_{a,x} \cdot m \cdot n_a + 2 \cdot k_{h,x}} \tag{13}$$

To ensure CP behaviour, the criterion is that the vertical reactions at the rotation points are positive (i.e., in compression). By establishing the dimensionless stiffness, $\tilde{k} = k_{h,z}/n \cdot k$, and dimensionless uniform vertical load, $\tilde{q} = (q \cdot m^2 \cdot b^2)/(2 \cdot F \cdot h)$, and after simplification, Equation (14) is obtained using vertical equilibrium of the first panel. This is considered for the first panel only since the other panels automatically meet the requirement when the reaction at the first panel is in compression and it is in contact with the ground. In this equation, γ_a is a ratio that accounts for the contribution of the multiple angle brackets, as expressed in Equation (15). If the vertical contribution of the angle brackets is desired to be omitted, it can be done by setting φ equal to zero.

$$\tilde{k} \geq \frac{1}{\left(1 + \frac{n_a}{2} \cdot \varphi\right)} \cdot \frac{1 - \frac{\tilde{q} \cdot (3 \cdot m - 2)}{m^2}}{1 - \frac{\tilde{q} \cdot (m - 2 \cdot \gamma_a)}{m^2}} \tag{14}$$

$$\gamma_a = \frac{1 + \alpha \cdot m \cdot \varphi}{1 + \frac{n_a}{2} \cdot \varphi} \tag{15}$$

2.3 Elastic analytical procedure to achieve SW behaviour

For the SW behaviour, the vertical displacements of the individual panels are different, however, the displacements due to rotation and sliding are the same as a result of the diaphragm constraint (Figure 3). The variables in the SW behaviour include rotation, ϑ, vertical displacement of each panel at the point of rotation, v_j, and the sliding displacement, Δ_s.

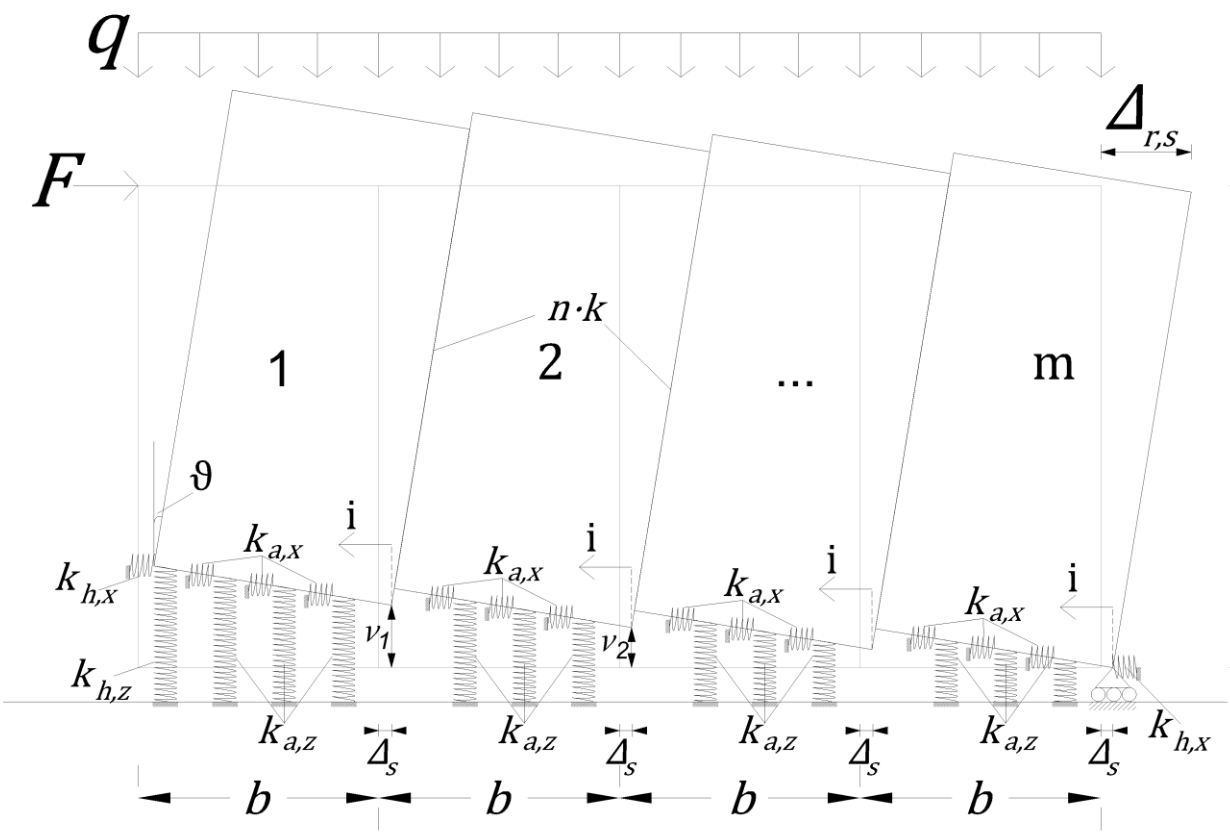

Figure 3: CLT multi-panel shear wall SW behaviour

Based on the deformed shape shown in Figure 3, the total potential energy of the wall assembly can be developed, as shown in Equation (16).

$$
\begin{aligned}
W_{total} = {} & \frac{1}{2} \cdot k_{h,z} \cdot \left\{ (v_1 + b \cdot \vartheta)^2 + \varphi \cdot \left[\alpha \cdot b^2 \cdot \vartheta^2 + \sum_{j=1}^{m-1} \sum_{i=1}^{n_a} \left(v_j + \frac{i}{(n_a + 1)} \cdot b \cdot \vartheta \right)^2 \right] \right\} \\
& + \frac{1}{2} \cdot n \cdot k \cdot \left[(b \cdot \beta \cdot \vartheta - v_{m-1})^2 + \sum_{j=1}^{m-2} \left(b \cdot \vartheta + v_{j+1} - v_j \right)^2 \right] + \frac{1}{2} \cdot \left(k_{a,x} \cdot n_a \cdot m + 2 \cdot k_{h,x} \right) \cdot {\Delta_s}^2 \\
& - F \cdot (h \cdot \vartheta + \Delta_s) + \frac{m \cdot q \cdot b^2 \cdot (2 \cdot \beta - 1)}{2} \cdot \vartheta + q \cdot b \cdot \sum_{j=1}^{m-1} v_j
\end{aligned}
\tag{16}
$$

Calculating the first derivative of Equation (16) provides expressions to solve for unknowns such as rotation and vertical displacement at the rotation center of each panel and sliding. Although by excluding the bi-axial effect of the angle brackets, one can obtain generalized solutions for the variables in the SW behaviour, including such contribution leads to different expressions that are dependent on the number of panels in the wall.

Equation (17) expresses the internal forces in each fastener in the vertical joints. It should be noted that in the SW behaviour, fasteners located in the same panel have equal internal force, same as CP, however, the internal forces of the vertical joints between different panels are not equal. Also, the effect of the compression zone only includes for the fasteners that join panel $m-1$ to m (i.e., $j=m-1$) since only panel m remains on the ground.

$$\begin{aligned} F_{c,y,j} &= k \cdot \left(b \cdot \vartheta + v_{j+1} - v_j\right), \qquad j = [1{:}\, m-2] \\ F_{c,y,j} &= k \cdot (b \cdot \beta \cdot \vartheta - v_{m-1}), \qquad j = m-1 \end{aligned} \tag{17}$$

The uplift force in the hold-down can be developed, as presented in Equation (18). The uplift force in the i^{th} angle bracket from the center of rotation in panel j, can be calculated using Equation (19). For the last panel ($j=m$), Equation (20) can be used given that v_m is equal to zero.

$$T_{h,z} = k_{h,z} \cdot (b \cdot \vartheta + v_1) \tag{18}$$

$$T_{a,i,j,z} = k_{a,z} \cdot \left(\frac{i}{n_a+1} \cdot b \cdot \vartheta + v_j\right), \qquad j = [1{:}\, m-1], i = [1{:}\, n_a] \tag{19}$$

$$T_{a,i,j,z} = k_{a,z} \cdot \left[\frac{i}{n_a+1} + (\beta - 1)\right] \cdot b \cdot \vartheta, \qquad j = m, i = [1{:}\, n_a] \tag{20}$$

Similar to the case presented for the CP behaviour, the horizontal forces in an angle bracket and hold-down can be obtained using Equations (12) and (13), respectively.

To illustrate the concept of the procedure for a simple system, an example is presented in

Equations (21)-(23) for $m = 2$ and $n_a = 3$, and $\beta = 1$. In this case, v_2 is equal to zero since in SW behaviour $m - 1$ panels displace vertically at the rotation point, while the last panel m is in contact with the ground. v_1 is the vertical displacement of the first panel at the rotation point, and ϑ is the rotation of the panels. The sliding displacement, Δ_s, can be obtained using Equation (7), by equating m to 2, as shown in Equation (23). The total lateral displacement at the top of the panels due to the sliding and rotation, $\Delta_{r,s}$, can be obtained using Equation (8).

$$\vartheta = \frac{2 \cdot \{F \cdot h \cdot [k_{h,z} \cdot (6 \cdot \varphi + 2) + 2 \cdot k \cdot n] - q \cdot b^2 \cdot (4 \cdot k \cdot n + 3 \cdot \varphi \cdot k_{h,z})\}}{b \cdot [\varphi \cdot k_{h,z}^2 \cdot (12 \cdot \varphi + 7) + k_{h,z} \cdot k \cdot n \cdot (31 \cdot \varphi + 16)]} \quad (21)$$

$$v_1 = \frac{-\{F \cdot h \cdot [k_{h,z} \cdot (6 \cdot \varphi + 4) - 4 \cdot k \cdot n] + q \cdot b^2 \cdot (8 \cdot k \cdot n + \varphi \cdot k_{h,z})\}}{b \cdot [\varphi \cdot k_{h,z}^2 \cdot (12 \cdot \varphi + 7) + k_{h,z} \cdot k \cdot n \cdot (31 \cdot \varphi + 16)]} \quad (22)$$

$$\Delta_s = \frac{F}{2 \cdot (3 \cdot k_{a,x} + k_{h,x})} \quad (23)$$

To ensure SW behaviour, the expression presented in Equation (24) needs to be satisfied, where the vertical displacement at the rotation point of panel $m - 1$ is required to be positive. This means that all panels except the last one would lift up and not maintain any contact with ground at the rotation point. This equation varies depending on the number of panels. An example is provided for $m = 2$ and $n_a = 3$ in Equation (25), by equating the vertical displacement at the rotation point for panel $m - 1$ (v_1) to zero. After simplification, this equation is rewritten, as shown in Equation (26).

$$v_{m-1} \geq 0 \quad (24)$$

$$F \cdot h \cdot [k_{h,z} \cdot (6 \cdot \varphi + 4) - 4 \cdot k \cdot n] + q \cdot b^2 \cdot (8 \cdot k \cdot n + \varphi \cdot k_{h,z}) \geq 0 \quad (25)$$

$$\tilde{k} < \frac{1 - \frac{\tilde{q}}{2}}{1 + \frac{\varphi}{2} \cdot \left(3 + \frac{\tilde{q}}{8}\right)}, \qquad for: m = 2, n_a = 3 \quad (26)$$

2.4 Inelastic analytical procedure

The elastic approach described in Section 2.2 is extended to the inelastic behaviour, including the effect of bi-axial contribution of the angle brackets and hold-downs. Similar methodology has been successfully used to describe the behaviour of CLT shearwalls with multiple panels [25], however these approaches omitted the vertical contribution of angle brackets and the horizontal effect of the hold-downs. The developed methodology focusses on the CP behaviour, because the CP behaviour is a desired final plastic behaviour since it promotes rocking kinematic mode [1, 20]. The CP plastic behaviour is attained when the vertical joints yield before the hold-down and angle brackets.

In the developed methodology outlined in this section, the connectors are assumed to behave as elastic-perfectly plastic. The properties used are: r_c, $r_{h,z}$, $r_{h,x}$, $r_{a,z}$ and $r_{a,x}$, representing the strength of the fasteners in the vertical joints, hold-downs in vertical and horizontal direction, and angle brackets in vertical and horizontal direction, respectively. Parameters d_y and d_u denote the yield and ultimate displacement of the connectors, respectively, with additional subscripts indicating the type of connector represented (i.e., c for fasteners in the vertical joints, hx and hz for hold-downs in horizontal and vertical directions, respectively, and ax and az for angle brackets in the horizontal and vertical directions, respectively).

The interaction between the vertical and horizontal direction in the angle brackets and hold-downs can be expressed in the circular domain, demonstrated in Equations (27) and (28), respectively, and shown in Figure 4 [26, 27]. In these equations, $T_{a,z}$ and $T_{a,x}$ are the internal forces in the angle brackets and $T_{h,z}$ and $T_{h,x}$ are the internal forces in the hold-downs.

$$\left(\frac{T_{a,z}}{r_{a,z}}\right)^2 + \left(\frac{T_{a,x}}{r_{a,x}}\right)^2 \leq 1.0 \qquad (27)$$

$$\left(\frac{T_{h,z}}{r_{h,z}}\right)^2 + \left(\frac{T_{h,x}}{r_{h,x}}\right)^2 \leq 1.0 \tag{28}$$

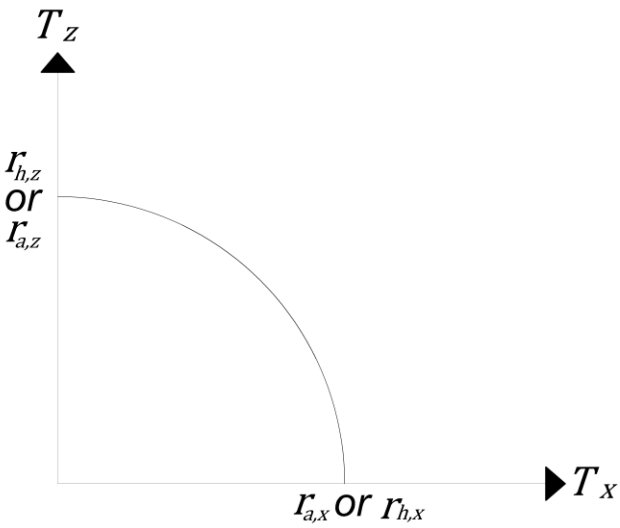

Figure 4: The circular domain representing the interaction effect of the angle brackets or hold-downs

The behaviour of the CLT shearwall in the elastic and inelastic regions is described in a generalized form in Figure 5. In Figure 5, P_0 represents the activation point at which the wall starts to rotate, corresponding to lateral force, R_{P_0}, and displacement, Δ_{P_0}. Points P_1 and P_2 represent the yielding of fasteners in the vertical joints and hold-down, respectively. Points P_3 to P_{n_a+2} represent the yielding order of the angle brackets starting from the last angle bracket away from the centre of rotation of each panel. The expression for the ultimate displacement of the shearwall is not established due to the uncertainty associated with the contribution of sliding and rotation after the yielding of all connections.

In the analytical procedure, a verification is made using Equations (27) and (28) to ensure that the angle brackets and hold-downs remain elastic. This verification is particularly important for the angle brackets because when the angle brackets start yielding, the wall is no longer capable of resisting additional horizontal loads, and consequently, it will proceed to slide until the ultimate failure in the angle brackets is reached.

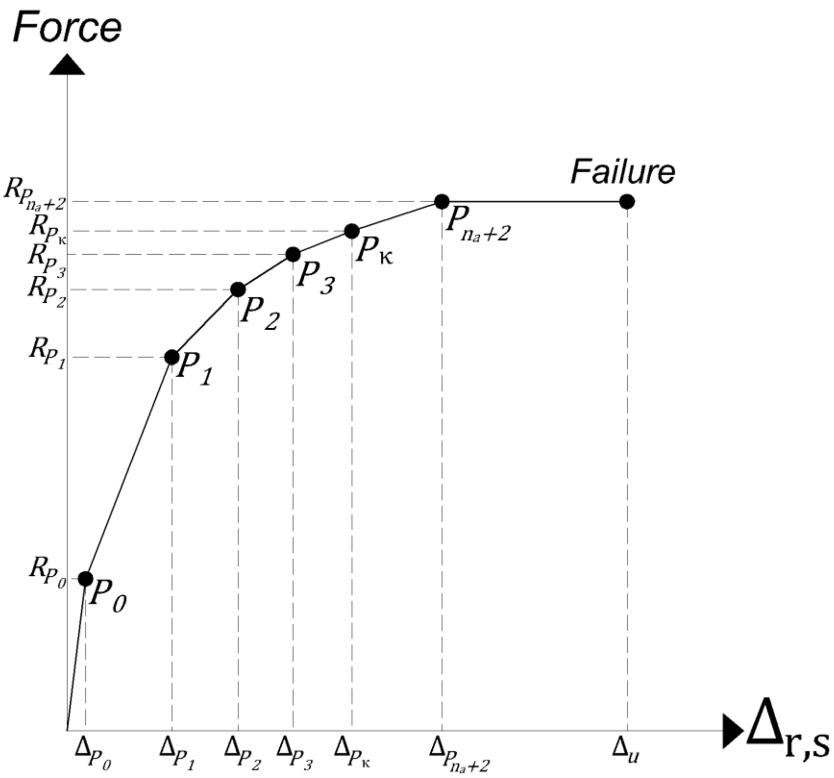

Figure 5: General inelastic diagram of multi-panel CLT shearwalls

The activation force, R_{P_0}, is defined as the lateral force at which the gravity load is overcome, and the panels start to rotate. The value of R_{P_0} can be obtained using Equation (29).

$$R_{P_0} = \frac{q \cdot m \cdot b^2 \cdot (2 \cdot \beta - 1)}{2 \cdot h} \tag{29}$$

At the activation force, the lateral displacement, Δ_{P_0}, is presented in Equation (30), using Equation (7). Since there is no rotation in the panels immediately prior to reaching the activation force, the lateral displacement is due to the sliding alone. Equations (31) and (32) are used to verify whether the angle brackets and hold-downs remain elastic. These equations are derived by setting the vertical component of the angle brackets and hold-downs, $T_{a,z}$ and $T_{h,z}$, in Equations (27) and (28) equal to zero, since there is no rotation or uplift in the panels.

$$\Delta_{P_0} = \frac{R_{P_0}}{k_{a,x} \cdot m \cdot n_a + 2 \cdot k_{h,x}} \tag{30}$$

$$0+\left(\frac{T_{a,x}}{r_{a,x}}\right)^2 < 1 \;\rightarrow\; \left[\frac{R_{P_0}\cdot k_{a,x}}{r_{a,x}\cdot\left(k_{a,x}\cdot m\cdot n_a+2\cdot k_{h,x}\right)}\right] < 1 \tag{31}$$

$$0+\left(\frac{T_{h,x}}{r_{h,x}}\right)^2 < 1 \;\rightarrow\; \left[\frac{R_{P_0}\cdot k_{h,x}}{r_{h,x}\cdot\left(k_{a,x}\cdot m\cdot n_a+2\cdot k_{h,x}\right)}\right] < 1 \tag{32}$$

The lateral force associated with the yielding of the fasteners in the vertical joints, denoted P_1 in Figure 5, can be expressed as presented in Equation (33). This expression is obtained by equating the elastic force in vertical joints, defined in Equation (9), with the yield capacity of the fasteners in the vertical joints, r_c. In this equation, $k'_{v,P_1} = k_v + (m-1)\cdot n\cdot k$, where k_v can be obtained from Equation (2).

$$R_{P_1} = \left(r_c\cdot\frac{k'_{v,P_1}\cdot b}{k\cdot h\cdot\beta}\right) + R_{P_0} \tag{33}$$

The associated lateral displacement due to the sliding and rocking, Δ_{P_1}, can be obtained using Equations (34), based on the elastic displacement of the wall in the CP behaviour, obtained from Equation (8). After simplification, Equation (35) is obtained as a function of yield displacement of fasteners in the vertical joints and sliding displacement. In Equation (34), K_{V,P_1} is the lateral stiffness of the shearwall at point P_1, obtained as $k'_{v,P_1}\cdot b^2/h^2$.

$$\begin{aligned}\Delta_{P_1} &= \left[\frac{R_{P_1}\cdot h^2}{b^2} - \frac{q\cdot m\cdot(2\cdot\beta-1)\cdot h}{2}\right]\cdot\frac{1}{k'_{v,P_1}} + \frac{R_{P_1}}{\left(k_{a,x}\cdot m\cdot n_a+2\cdot k_{h,x}\right)} \\ &= \frac{R_{P_1}-R_{P_0}}{K_{V,P_1}} + \frac{R_{P_1}}{\left(k_{a,x}\cdot m\cdot n_a+2\cdot k_{h,x}\right)}\end{aligned} \tag{34}$$

$$\Delta_{P_1} = d_{y,c}\cdot\frac{h}{b\cdot\beta} + \frac{R_{P_1}}{\left(k_{a,x}\cdot m\cdot n_a+2\cdot k_{h,x}\right)} \tag{35}$$

The internal uplift force in the angle brackets and hold-down at the point of yielding of the vertical joints, $T_{a,z}^{P_1}$ and $T_{h,z}^{P_1}$, are presented in Equations (36) and (37), respectively. These equations are based on the elastic uplift load in the angle brackets and hold-down and where F is replaced by the associated lateral load at this point, equal to R_{P_1}.

$$T_{a,z,i}^{P_1} = \left[\frac{i}{n_a+1} + (\beta - 1)\right] \cdot \left[\frac{R_{P_1} \cdot h}{b^2} - \frac{q \cdot m \cdot (2 \cdot \beta - 1)}{2}\right] \cdot \frac{\varphi \cdot k_{h,z} \cdot b}{k'_{v,P_1}}, \quad i = [1 : n_a] \tag{36}$$

$$T_{h,z}^{P_1} = \left[\frac{R_{P_1} \cdot h}{b^2} - \frac{q \cdot m \cdot (2 \cdot \beta - 1)}{2}\right] \cdot \frac{k_{h,z} \cdot b \cdot \beta}{k'_{v,P_1}} \tag{37}$$

At this point, the angle brackets and hold-downs remain in the elastic region if the interaction expression outlined in Equation (38) and (39) are satisfied. These equations are based on the general interaction equation (i.e., Equation (27) and (28)), while replacing the associated internal forces using the equations provided in section 2.2.

$$\left(\frac{T_{a,z,i}^{P_1}}{r_{a,z}}\right)^2 + \left[\frac{R_{P_1} \cdot k_{a,x}}{r_{a,x} \cdot \left(k_{a,x} \cdot m \cdot n_a + 2 \cdot k_{h,x}\right)}\right]^2 < 1.0, \qquad i = [1 : n_a] \tag{38}$$

$$\left(\frac{T_{h,z}^{P_1}}{r_{h,z}}\right)^2 + \left[\frac{R_{P_1} \cdot k_{h,x}}{r_{h,x} \cdot \left(k_{a,x} \cdot m \cdot n_a + 2 \cdot k_{h,x}\right)}\right]^2 < 1.0 \tag{39}$$

The increase in the internal hold-down force from P_1 to P_2, $t_{h,z}^{P_2}$, can be obtained by replacing F in the internal forces of hold-down with the associated increase in lateral force, $R_{P_2} - R_{P_1}$. The lateral load capacity of the shearwall at point P_2, representing the yield point of the hold-down, is denoted R_{P_2}. In Equation (40), k'_{v,P_2} is equal to k_v, since the vertical joints have yielded and are no longer contributing to the wall stiffness. It is noteworthy to mention that the effect of uniform load q is not considered in the equations developed subsequently, since such effect has already been taken into account in the equations at point P_1 and P_0.

$$t_{h,z}^{P_2} = \left[\frac{\left(R_{P_2} - R_{P_1}\right) \cdot h}{b}\right] \cdot \frac{k_{h,z}}{k'_{v,P_2}} = \frac{\left(R_{P_2} - R_{P_1}\right) \cdot h \cdot \beta}{b \cdot (\beta^2 + \alpha \cdot \varphi \cdot m)} \tag{40}$$

By equating the interaction expression for the hold-down at P_2 to 1, as shown in Equation (41), the lateral capacity at this level, R_{P_2}, can be obtained. The solution to this equation is cumbersome and is more suitable for use in the development of software solutions, especially for higher number of panels.

The associated uplift force in the hold-down, $T_{h,z}^{P_2}$, is equal to the sum of $T_{h,z}^{P_1}$ and $t_{h,z}^{P_2}$.

$$\left(\frac{T_{h,z}^{P_2}}{r_{h,z}}\right)^2 + \left[\frac{R_{P_2} \cdot k_{h,x}}{r_{h,x} \cdot \left(k_{a,x} \cdot m \cdot n_a + 2 \cdot k_{h,x}\right)}\right]^2 = 1.0 \qquad (41)$$

The increase in lateral displacement from P_1 to P_2, δ_{P_2}, can be determined using Equation (42). This equation is based on the elastic displacement obtained in the CP behaviour, Equation (8), by replacing the lateral load, F, with the associated increase in lateral load capacity, $R_{P_2} - R_{P_1}$. Finally, the lateral displacement at P_2 due to the sliding and rocking is presented in Equation (43), which can be obtained by summing the lateral displacement at P_1, Δ_{P_1}, and the increase in lateral displacement, δ_{P_2}. The lateral stiffness of shearwalls at P_2, K_{V,P_2}, is defined as $k'_{v,P_2} \cdot b^2/h^2$.

$$\begin{aligned}\delta_{P_2} &= \left[\frac{\left(R_{P_2} - R_{P_1}\right) \cdot h^2}{b^2}\right] \cdot \frac{1}{k'_{v,P_2}} + \frac{R_{P_2} - R_{P_1}}{\left(k_{a,x} \cdot m \cdot n_a + 2 \cdot k_{h,x}\right)} \\ &= \frac{R_{P_2} - R_{P_1}}{K_{V,P_2}} + \frac{R_{P_2} - R_{P_1}}{\left(k_{a,x} \cdot m \cdot n_a + 2 \cdot k_{h,x}\right)}\end{aligned} \qquad (42)$$

$$\Delta_{P_2} = \Delta_{P_1} + \delta_{P_2} = d_{y,c} \cdot \frac{h}{b \cdot \beta} + \frac{R_{P_2} - R_{P_1}}{K_{V,P_2}} + \frac{R_{P_2}}{\left(k_{a,x} \cdot m \cdot n_a + 2 \cdot k_{h,x}\right)} \qquad (43)$$

To ensure that the fasteners in the vertical joints do not reach their ultimate displacement at or before P_2, Equation (44) is required to be satisfied.

$$d_{y,c} + \frac{b \cdot \beta}{h} \cdot \frac{R_{P_2} - R_{P_1}}{K_{V,P_2}} < d_{u,c} \qquad (44)$$

The increase in internal uplift force in the i^{th} angle brackets from P_1 to P_2, $t_{a,z}^{P_2}$, is presented in Equation (45):

$$t_{a,z,i}^{P_2} = \left[\frac{i}{n_a + 1} + (\beta - 1)\right] \cdot \left[\frac{\left(R_{P_2} - R_{P_1}\right) \cdot h^2}{b^2}\right] \cdot \frac{\varphi \cdot k_{h,z} \cdot b}{k'_{v,P_2} \cdot h} \qquad (45)$$

$$= \left[\frac{i}{n_a + 1} + (\beta - 1)\right] \cdot \frac{\left(R_{P_2} - R_{P_1}\right) \cdot h \cdot \varphi}{b \cdot (\beta^2 + \alpha \cdot \varphi \cdot m)}, \qquad i = [1{:}\, n_a]$$

At this point, the vertical uplift load in the angle brackets is obtained as the sum of Equation (45) and (36). Also, the horizontal load in the angle brackets can be obtained using Equation (12). Equation (46) is used to check that the angle brackets remain in elastic region. It is only required to check the last angle brackets from the centre of rotation of each panel ($i = n_a$).

$$\left(\frac{T_{a,z,n_a}^{P_1} + t_{a,z,n_a}^{P_2}}{r_{a,z}}\right)^2 + \left[\frac{R_{P_2} \cdot k_{a,x}}{r_{a,x} \cdot \left(k_{a,x} \cdot m \cdot n_a + 2 \cdot k_{h,x}\right)}\right]^2 < 1.0 \tag{46}$$

Equation (47) represents the increase in the uplift forces in the angle brackets after the yielding of the vertical joints and the hold-down. The increase in the vertical uplift force in the angle brackets from $P_{\kappa-1}$ to P_κ, is denoted as $t_{a,z,i}^{P_\kappa}$, where κ is equal to $[3{:}\, n_a + 2]$. Equation (48) represents the contribution to stiffness of those angle brackets that remain elastic in the uplift direction at P_κ, k'_{v,P_κ}. In this equation, f is equal to $(n_a + 3) - \kappa$.

$$t_{a,z,i}^{P_\kappa} = \left[\frac{i}{n_a + 1} + (\beta - 1)\right] \cdot \left[\frac{\left(R_{P_\kappa} - R_{P_{\kappa-1}}\right) \cdot h}{b^2}\right] \cdot \frac{\varphi \cdot k_{h,z} \cdot b}{k'_{v,P_\kappa}}, \qquad i = [1{:}\, f] \tag{47}$$

$$k'_{v,P_\kappa} = k_{h,z} \cdot \varphi \cdot m \cdot \sum_{i=1}^{f} \left[\frac{i}{(n_a + 1)} + (\beta - 1)\right]^2 \tag{48}$$

In order to determine the yield point of the associated angle brackets, Equation (49) is obtained by equating the interaction equation (i.e., Equation (27)) to 1. The associated lateral capacity, R_{P_κ}, can be obtained by solving this equation, however similar to Equation (41), the solution to this equation is cumbersome and does not lend itself to reasonable simple expressions, especially for higher number of panels.

$$\left(\frac{T_{a,z,f}^{P_1} + t_{a,z,f}^{P_2} + \sum_{x=3}^{\kappa} t_{a,z,f}^{P_x}}{r_{a,z}}\right)^2 \tag{49}$$

$$+\left\{\frac{1}{r_{a,x}}\cdot\left[\frac{R_{P_2}\cdot k_{a,x}}{\left(k_{a,x}\cdot m\cdot n_a+2\cdot k_{h,x}\right)}+\sum_{x=3}^{\kappa}\frac{\left(R_{P_x}-R_{P_{x-1}}\right)\cdot k_{a,x}}{m\cdot k_{a,x}(n_a+3-x)+k_{h,x}}\right]\right\}^2=1.0$$

The increase in the lateral displacement from $P_{\kappa-1}$ to P_κ, δ_{P_κ}, can be derived using the same procedure as described for Equation (42), by considering the associated increase in the lateral load capacity, as expressed in Equation (50). The lateral displacement due to sliding and rocking, Δ_{P_κ}, can be calculated using Equation (51), which is the sum of the total lateral displacement at $P_{\kappa-1}$, and the increase in the displacement from $P_{\kappa-1}$ to P_κ, obtained using Equation (50). K_{V,P_κ} is defined as $k'_{v,P_\kappa}\cdot b^2/h^2$.

$$\begin{aligned}\delta_{P_\kappa}&=\left[\frac{\left(R_{P_\kappa}-R_{P_{\kappa-1}}\right)\cdot h^2}{b^2}\right]\cdot\frac{1}{k'_{v,P_\kappa}}+\frac{R_{P_\kappa}-R_{P_{\kappa-1}}}{k_{a,x}\cdot m\cdot f+k_{h,x}}\\&=\frac{R_{P_\kappa}-R_{P_{\kappa-1}}}{K_{V,P_\kappa}}+\frac{R_{P_\kappa}-R_{P_{\kappa-1}}}{k_{a,x}\cdot m\cdot f+k_{h,x}}\end{aligned}\tag{50}$$

$$\Delta_{P_\kappa}=\Delta_{P_{\kappa-1}}+\delta_{P_\kappa}=\Delta_{P_{\kappa-1}}+\frac{R_{P_\kappa}-R_{P_{\kappa-1}}}{K_{V,P_\kappa}}+\frac{R_{P_\kappa}-R_{P_{\kappa-1}}}{k_{a,x}\cdot m\cdot f+k_{h,x}}\tag{51}$$

At P_κ, it is required to ensure that the fasteners in the vertical joints have not reached their respective ultimate displacements by satisfying Equation (52).

$$d_{y,c}+\frac{b\cdot\beta}{h}\cdot\sum_{i=2}^{\kappa}\frac{R_{P_i}-R_{P_{i-1}}}{K_{V,P_i}}<d_{u,c}\tag{52}$$

To ensure that the hold-down connections do not reach their ultimate displacement at P_κ, Equation (53) needs to be satisfied. In this equation, Δ_{s,P_κ} and D_{z,P_κ} are the sliding and uplift displacement in the hold-down, respectively, as presented in Equations (54) and (55).

$$\left(\frac{D_{z,P_\kappa}}{d_{u,hz}}\right)^2+\left(\frac{\Delta_{s,P_\kappa}}{d_{u,hx}}\right)^2<1\tag{53}$$

$$\Delta_{s,P_\kappa}=\frac{R_{P_2}}{\left(k_{a,x}\cdot m\cdot n_a+2\cdot k_{h,x}\right)}+\sum_{i=3}^{\kappa}\frac{R_{P_i}-R_{P_{i-1}}}{k_{a,x}\cdot m\cdot(n_a+3-i)+k_{h,x}}\tag{54}$$

$$D_{z,P_\kappa} = d_{y,c} + \frac{b \cdot \beta}{h} \cdot \sum_{i=2}^{\kappa} \frac{R_{P_i} - R_{P_{i-1}}}{K_{V,P_i}} \tag{55}$$

It is required to ensure that the last angle bracket from the centre of rotation of each panel, which has the highest uplift force, does not reach its ultimate displacement, as presented in Equation (56). This equation is expected to be checked for values of κ greater than 3, since for values equal or less than 3, the angle brackets would not have started to yield.

$$\left\{\left[\frac{n_a}{n_a + 1} - (1 - \beta)\right] \cdot \frac{D_{z,P_\kappa}}{d_{u,az} \cdot \beta}\right\}^2 + \left(\frac{\Delta_{s,P_\kappa}}{d_{u,ax}}\right)^2 < 1 \tag{56}$$

2.5 Shear deformation in CLT shear walls

The CLT panels have so far been assumed as rigid bodies and as such their shear deformation has been ignored in the development of the proposed model. The shear deformation contribution of the panels can be independently calculated and then incorporated into the total lateral deformation equation containing the lateral displacements due to rocking and sliding [28]. The shear deformation of panel j, $\Delta_{sh,j}$, can be calculated using the expression presented in Equation (57). In this equation, F_j is the lateral load in the j^{th} panel, G is the equivalent shear modulus, which can be obtained using the equation proposed by Brandner et al. [29], and t is the thickness of CLT panels.

$$\Delta_{sh,j} = \frac{F_j \cdot h}{G \cdot t \cdot b}, \qquad j = [1 : m] \tag{57}$$

By incorporating the sum of shear deformation from all the CLT panels into the lateral displacement due to the rocking and sliding proposed from sections 2.2-2.4., one obtains the expression in Equation (58) for the total lateral displacement of the CLT shearwall, Δ_{total}.

$$\Delta_{total} = \Delta_r + \Delta_s + \sum_{j=1}^{m} \Delta_{sh,j} \tag{58}$$

3. The influence of angle brackets

3.1 Kinematic consistency regions

The kinematic regions, depicting areas where different kinematic modes govern the behaviour of the wall, are plotted using the consistency (limit) expressions provided in Equations (14) and (24) for the CP and SW behaviour, respectively. The IN region can be obtained as the area between the CP and SW behaviours. The graphs are based on the dimensionless vertical load, $\tilde{q}$, and dimensionless stiffness, $\tilde{k}$, allowing for the representation of different properties of connectors and applied loads. The angle brackets stiffness ratio, φ, is considered for discrete values of 0, 0.5 and 1. An example of such representation is demonstrated in Figure 6, for shearwalls consisting of 4 and 6 panels with one angle bracket at the middle of each panel (i.e., $n_a = 1$), while also neglecting the compression zone (i.e., $\beta = 1$) for simplicity.

As expected, when the bi-axial effect of the angle brackets is considered in the analysis, especially for relatively stiff angle brackets in vertical direction (i.e., large values of φ), more panels are likely to maintain contact with the ground, resulting in less displacements and rotations. Comparing Figure 6-a (depicting 4 panels) to Figure 6-b (depicting 6 panels), it can be observed that as the number of panels increases, the SW region becomes smaller for all values of φ, since more connectors are involved in resisting the vertical uplift load, resulting in a stronger and stiffer wall assembly.

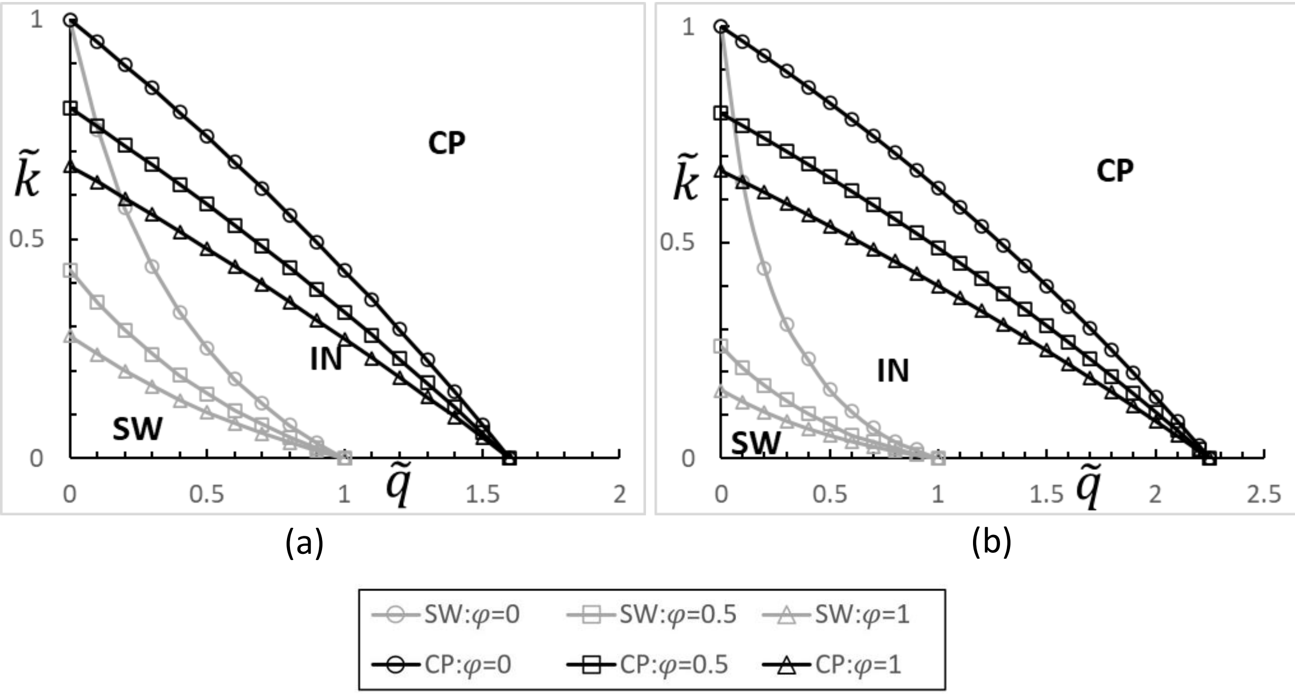

Figure 6: The consistency regions for CLT shearwalls a) $m = 4$ b) $m = 6$

For the case with no vertical load ($\tilde{q} = 0$), it can be observed that when the bi-axial behaviour of angle brackets is neglected ($\varphi = 0$), either CP or SW behaviour is attained for $\tilde{k}$ values greater than or lesser than 1, respectively, independent of the number of panels. However, when the vertical contribution of angle brackets is considered, the SW region is smaller for larger values of φ, and all three kinematic modes (CP, SW, and IN) are possible.

By increasing the dimensionless vertical load, $\tilde{q}$, the difference between the boarder lines for both CP and SW becomes smaller. This implies that the influence of the vertical contribution of angle brackets on the overall wall behaviour is less significant when the gravity load increases. It can be observed that at the SW limit, the boarder lines coincide at a value of $\tilde{q}$ equal to 1, irrespective of the number of panels (Figure 6), which means that for $\tilde{q} > 1$, the SW behaviour cannot be attained. For the CP behaviour, the boarder lines coincide at a $\tilde{q}$ value that depends on the number of panels, number of fasteners in the vertical joints and the geometry of panels.

When $\tilde{k}$ exceeds a limit value, CP behaviour can be achieved regardless of the value of $\tilde{q}$ and of the number of panels. This limit is equal to 1 ($\tilde{k} > 1$), for the case where the bi-axial effect of angle brackets is neglected. For the case where angle brackets with high vertical stiffness is considered ($\varphi = 1$) the limit value is obtained by equating the vertical uniform load, q, to zero based on the CP limit equation (Equation (14)), yielding a value of 0.67 ($\tilde{k} > 0.67$).

3.2 Sensitivity analysis

Sensitivity analyses are carried out to investigate the contribution of the vertical stiffness of the angle brackets, considering the developed elastic analytical expressions for values of $\tilde{k}$ between 0 and 1.5. This is done by varying the vertical stiffness of hold-down and maintaining constant stiffness and number of fasteners in the vertical joints, while assuming only one angle bracket at the middle of each panel. The analysis is repeated for a range of angle brackets' stiffness ratios, φ, between 0.25 to 1, and the results are compared to the reference case where the angle bracket stiffness is neglected ($\varphi = 0$). The analyses are conducted for number of panels equal to 4 and 8, and for a constant height and width of panels equal to 2.7 m and 1.4 m, respectively. Different $\tilde{q}$ values are considered (0, 1, 2 and 3.5), depending on the number of panels, in order to evaluate all possible kinematic modes (i.e., CP, SW and IN). The parameters used in sensitivity analysis are summarized in Table 1.

Table 1: The input of sensitivity analysis

Parameter	Value(s)/range
$\tilde{k}$	0 to1.5
$\tilde{q}$	0,1,2,3.5
φ	0.25,0.5,0.75,1
n	18
n_a	1
$k\ (KN/m)$	700
$k_{h,z}\ (KN/m)$	variable
$h\ (m)$	2.7
$b\ (m)$	1.4

The parameters studied include panel rotation (ϑ) and internal forces in hold-down in the vertical direction as well as fasteners in the vertical joints ($T_{h,z}$ and $F_{c,y,j}$, respectively). In the CP region, the internal forces in the connectors are related linearly to the rotations, as concluded by considering Equations (9)-(11). For this reason, all the studied parameters are expected to have the same trends and are expressed as the same variable, x (i.e., ϑ, $T_{h,z}$ and $F_{c,y,j}$). On the contrary, for the SW region all three parameters are independent and therefore investigated separately. $\rho(x)$ expresses the ratio of the parameters studied (x) when the bi-axial effect of the angle brackets is neglected, $x_{\varphi=0}$, and considered, $x_{\varphi>0}$, as presented in Equation (59).

$$\rho(x) = \frac{x_{\varphi=0}}{x_{\varphi>0}} \tag{59}$$

Figure 7 presents the sensitivity analysis results for a 4 panel CLT shearwall with no uniform vertical load ($\tilde{q} = 0$), where all three possible behaviours can be achieved. The ratio of rotation, uplift forces in the hold-down and forces in the vertical joints are presented in Figure 7-a, Figure 7-b and Figure 7-c, respectively.

The results of rotation and vertical forces in the hold-down show almost the same trend, where the highest effect is observed in the SW region, while in the CP region, the effect is relatively less significant. The internal forces in vertical joints are almost unaffected by the vertical stiffness of the angle brackets for all regions, especially the SW region.

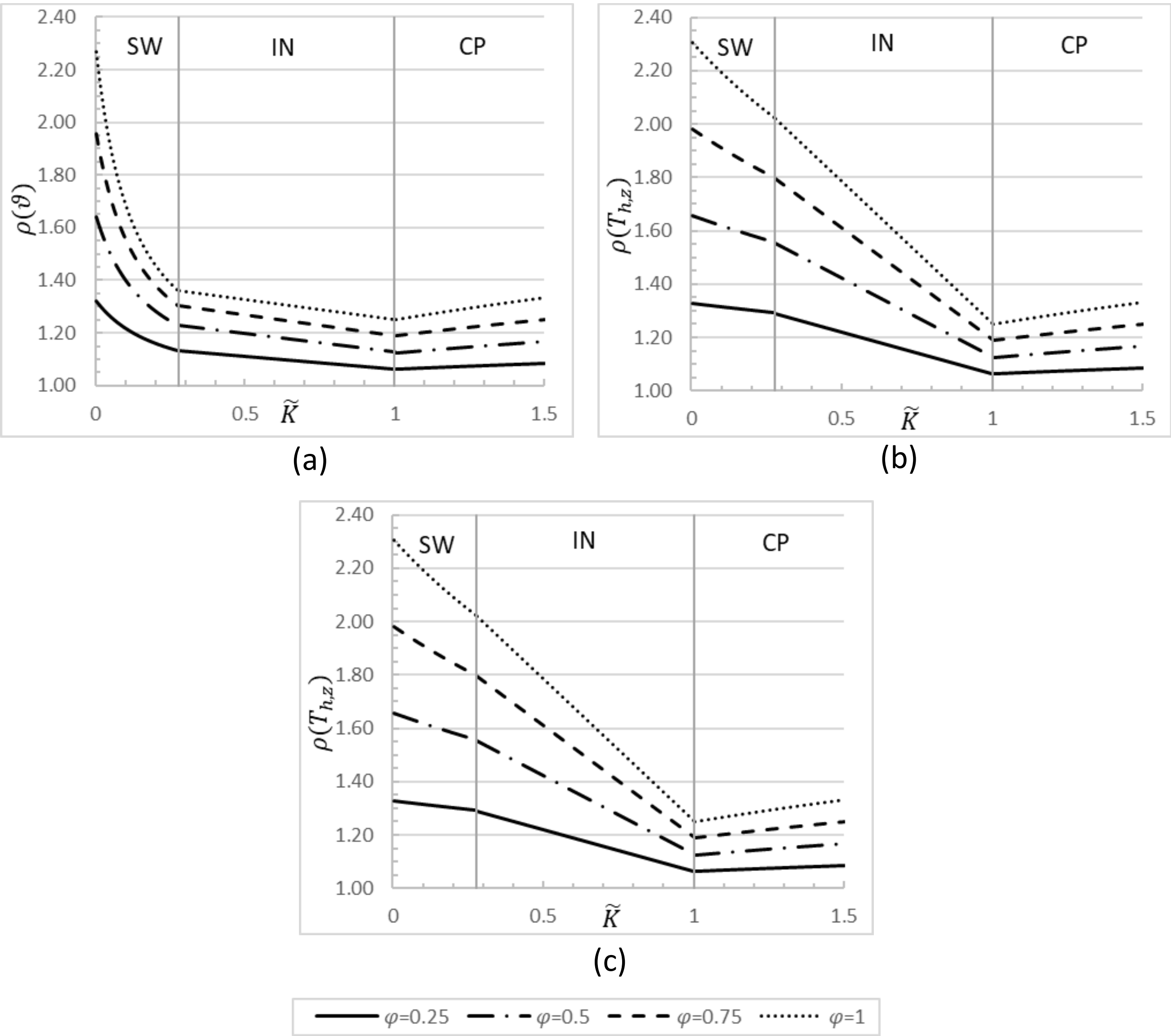

Figure 7: Sensitivity analysis for 4th panel CLT shearwalls for $\tilde{q} = 0$: a) rotation b) Hold-down vertical forces c) Vertical joints' forces

Figure 8 compares the results of the sensitivity analyses in the CP and SW behaviour for CLT shearwalls consisting of 4 and 8 panels. In order to maintain the CP behaviour, Figure 8-a), a value of $\tilde{q}$ was selected to be 2.0 and 3.5 for walls with 4 and 8 panels, respectively. For the SW behaviour, (Figure 8-b), $\tilde{q}$ was set equal to 0 and the results are shown for the uplift forces in hold-down for which the most differences are observed. It can be observed that the effect of the number of panels seems insignificant in CP. On the contrary, significant differences are observed in the SW when the number of panels are considered doubled.

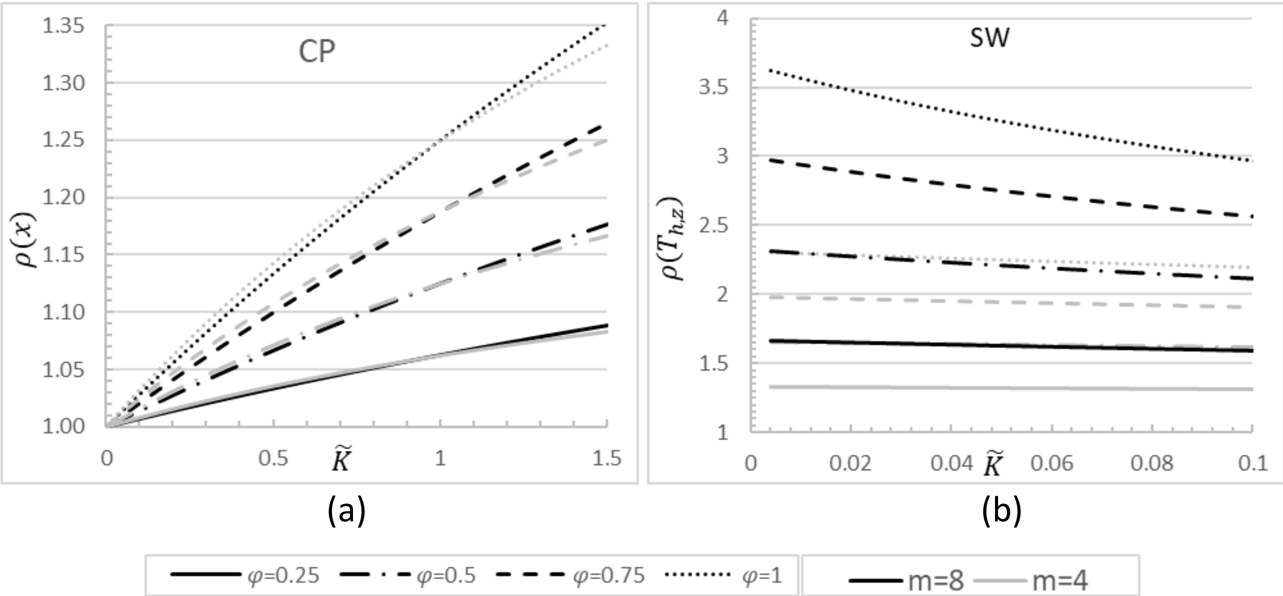

Figure 8: Sensitivity analysis for the 4th and 8th panels CLT shearwall a) CP behaviour b) SW behaviour

In order to measure the effect of multiple angle brackets in CP, a new variable, ∅, is defined, as shown in Equation (60). In this equation, α and φ can be obtained using Equations (1) and (3), respectively.

$$\emptyset = \alpha \cdot \varphi \tag{60}$$

The results of the sensitivity analyses in the CP behaviour are summarized in Table 2. The analyses are conducted for values of $\tilde{k}$ equal to 0.5, 1 and 3.5, and values of $\tilde{q}$ equal to 0, 1, 2 and 3.5. To investigate the effect of multiple angle brackets, different values of ∅ between 0.125 and 1, are adopted. As seen in the table, varying $\tilde{k}$ seems to have a relatively small impact on the results. Comparing the differences of considering and neglecting the contribution of the angle brackets for different values of $\tilde{q}$, it can be observed that identical values are obtained. Figure 8 shows that for ∅ values equal to 0.125 and 0.25, the greatest ratio observed is 1.17 and 1.33, respectively. This observation has a significant implication on the analysis and design of CLT shearwalls, and whether the bi-axial effect of the angle brackets need to be considered. Based on the results of this study, it can be concluded that the biaxial contribution of the angle brackets may be neglected if relatively flexible angle brackets are used ($\emptyset < 0.125$) in the CP behaviour. In those cases, a maximum difference of 17% or less is obtained. However, in the case with relatively stiff angle brackets or when multiple angle brackets with significant stiffness ($\emptyset = 1$) are used, it is observed that the bi-axial effect of the angel brackets is significant, in the range of 53 to 141%. Also, it should be noted, that if the SW behaviour is attained, considering the bi-axial effect of angle brackets is required since neglecting such effect would lead to errors of more than 20%.

Table 2: The results of sensitivity analysis for CP behaviour

		$\tilde{q} = 0$			$\tilde{q} = 1$			$\tilde{q} = 2$			$\tilde{q} = 3.5$		
		$\tilde{k}$			$\tilde{k}$			$\tilde{k}$			$\tilde{k}$		
		0.5	1	1.5	0.5	1	1.5	0.5	1	1.5	0.5	1	1.5
Num. of panels	∅	$\rho(x)$			$\rho(x)$			$\rho(x)$			$\rho(x)$		
4	0.125	N.A.	1.13	1.17	1.07	1.13	1.17	1.07	1.13	1.17	1.07	1.13	1.17
	0.25	N.A.	1.25	1.33	1.14	1.25	1.33	1.14	1.25	1.33	1.14	1.25	1.33
	0.375	N.A.	1.38	1.5	1.21	1.38	1.5	1.21	1.38	1.5	1.21	1.38	1.5
	0.5	N.A.	1.50	1.67	1.29	1.50	1.67	1.29	1.50	1.67	1.29	1.50	1.67
	0.75	N.A.	1.75	2	1.43	1.75	2	1.43	1.75	2	1.43	1.75	2
	1	N.A.	2	2.33	1.57	2	2.33	1.57	2	2.33	1.57	2	2.33
8	0.125	N.A.	1.13	1.18	N.A.	1.13	1.18	1.07	1.13	1.18	1.07	1.13	1.18
	0.25	N.A.	1.25	1.35	N.A.	1.25	1.35	1.13	1.25	1.35	1.13	1.25	1.35
	0.375	N.A.	1.38	1.53	N.A.	1.38	1.53	1.2	1.38	1.53	1.2	1.38	1.53
	0.5	N.A.	1.5	1.71	N.A.	1.5	1.71	1.27	1.5	1.71	1.27	1.5	1.71
	0.75	N.A.	1.75	2.06	N.A.	1.75	2.06	1.4	1.75	2.06	1.4	1.75	2.06
	1	N.A.	2	2.41	N.A.	2	2.41	1.53	2	2.41	1.53	2	2.41

4. Verification of the proposed methods

The proposed methodologies are verified using commercially available analysis software

(SAP2000) [30] and validated against experimental tests results obtained from the literature [21].

4.1. Verification of the method with numerical model

In order to ensure that the proposed analysis procedure is mathematically correct, a general example is presented for the inelastic range. In this example, the following input parameters are assumed: the elastic mechanical properties for the hold-down stiffness in the vertical and horizontal directions, $k_{h,z}$ and $k_{h,x}$, are assumed equal to 5700 KN/m and 2000 KN/m, respectively, the angle brackets' stiffness ratio, φ, is set equal to 0.5, the horizontal stiffness of angle brackets, $k_{a,x}$, is equal to 2600 KN/m, and the stiffness of the fasteners in the vertical joints, k, is equal to 700 KN/m. The number of panels (m) and number of fasteners in each vertical joint (n) are taken as 3 and 18, respectively. Also, for simplicity, values related to the number of angle brackets and compression zone of $n_a = 1$ and $\beta = 1$ are assumed.

The inelastic behaviour of the connectors is modelled using bi-linear springs. The properties of the variables used are summarized in Table 3. This verification is meant to illustrate the trend of the generalised diagram (Figure 5), considering the ultimate displacements of connectors set to infinity. The analysis is undertaken until 50 mm lateral displacement in the shearwall is achieved.

Table 3: Inelastic properties used in inelastic verification

$\boldsymbol{r_{h,Z}}$	$\boldsymbol{r_C}$	$\boldsymbol{r_{a,x}}$	$\boldsymbol{r_{a,z}}$	$\boldsymbol{d_{y,hz}}$	$\boldsymbol{d_{y,c}}$	$\boldsymbol{d_{y,az}}$	$\boldsymbol{d_{y,ax}}$	$\boldsymbol{d_{u,hz}}$	$\boldsymbol{d_{u,c}}$	$\boldsymbol{d_{u,az}}$	$\boldsymbol{d_{u,ax}}$
30	2.8	40	20	5.25	4	7	15.2	Inf.	Inf.	Inf.	Inf.

The results obtained from the inelastic analysis are shown in Figure 9. As can be seen, the analytical solution matches that obtained from the numerical model almost perfectly. This comparison reflects the mathematical accuracy of the proposed model and shows that for a general case the match between the proposed analytical method and the numerical analysis can be obtained with reasonable accuracy.

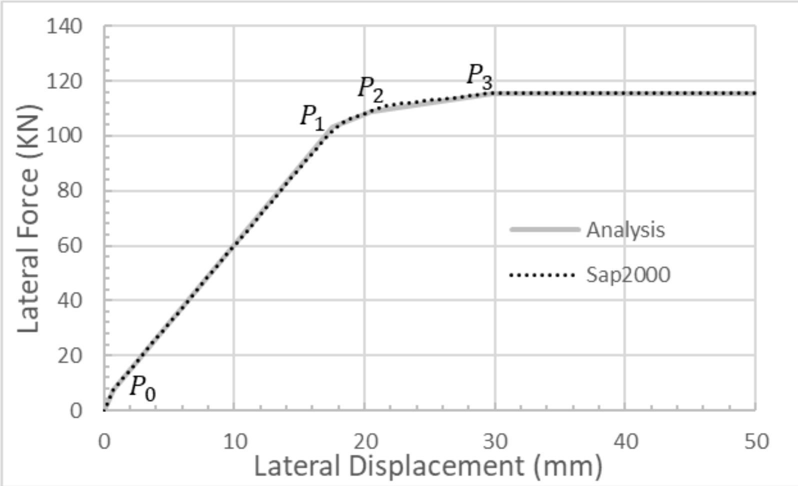

Figure 9: The inelastic results of analytical and numerical models

4.2. Validation of the method with published experimental results

The methods proposed in this paper are validated by comparing the results from the analytical model with experimental results obtained from [21]. Four examples of two-panel CLT shearwalls in the CP behaviour were investigated, using the same mechanical properties and configurations as those used in the tests. Table 4 presents the mechanical properties of the connectors, including yield strength, r, stiffness, k, yield displacement, d_y, and ultimate displacement, d_u, obtained by idealizing the connection behaviour as elastic-perfectly plastic, using the EEEP methods outlined in the ASTM E2126 [31] standard. The hold-downs are assumed elastic in the horizontal direction, and for simplicity, the compression zone is neglected ($\beta = 1$).

Table 4: Mechanical properties of connectors obtained from experiments in [21]

Connectors	$r\ (KN)$	$k\ (KN/m)$	$d_y\ (mm)$	$d_u\ (mm)$
Hold-down, z	44.41	4592	9.67	23.75
Hold-down, x	-	3195	-	-
Angle brackets, z	21.36	2647	8.07	23.19
Angle brackets, x	24.9	1958	12.72	31.86
Vertical joints, a	4.33	1267	3.42	31.55

Vertical joints, b	6.15	851	7.23	37.66

Table 5 provides details summarizing the configurations of the experimental wall specimens used in the comparison. This includes the number of vertical joints and angle brackets in each panel, the number of hold-downs, and the type of fasteners used in the vertical joints. Vertical joints a and b consisted of half-lap and spline joint with laminated veneer lumber (LVL), respectively (see Table 5 and Figure 10-a and -b). Figure 10-c illustrates the wall configuration, including spaces between anchors and overall dimensions of the panels.

Table 5: General information about the experimental configurations

Examples	Number of fasteners per vertical joint (n)	Type of fasteners in Vertical joints	Number of angle brackets (n_a)	Number of hold-downs on each side of the wall	Failure modes
1	10	a	2	1	CP
2	5	a	2	2	CP
3	10	b	2	1	CP
4	5	b	2	2	CP

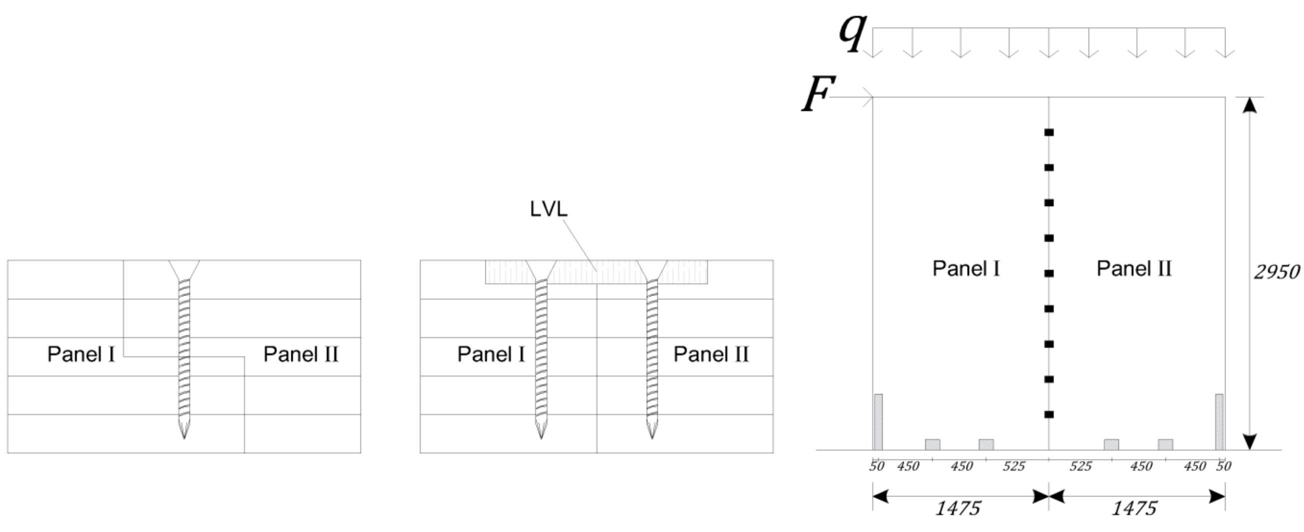

(a) (b) (c)

Figure 10: a) half-lap joint; b) spline LVL joint; c) tested wall configuration (the unit is mm)

The complete force-displacement curves for the experimental results could not be obtained from the original study since what is reported is only an idealization of the continuous curves using tri-linear curves. A comparison between the results obtained from the reported experimental study [21] and those from the proposed model can be seen in Figure 11. It can be observed that a reasonable fit is obtained between the proposed model and the experimental results, particularly related to the peak load. It is difficult to directly compare the initial stiffness and the yield points, due to the idealization of the experimental curves (i.e. using a tri-linear curve), however, it can be seen that the general shape of the curves is consistent and matches reasonably well. It is noteworthy to mention that the model developed in this study is not capable of predicting the post-peak behaviour of the shearwalls due to the idealization made regarding the behaviour of the hold-down and angle bracket connection being elastic-perfectly plastic. In an attempt to quantify the error in the prediction, Table 6 presents the ratio between the peak lateral forces, $F_{max,ex}/F_{max,an}$, and elastic stiffness, K_{ex}/K_{an}, obtained from the experimental and analytical methods. K_{ex} represents the slope of the initial line of the tri-linear curve obtained from the experimental results and K_{an} is obtained using the EEEP procedure outlined in [31] on the multi-linear analytical curves obtained from the proposed model. It should be noted that the ultimate displacement cannot be predicted using the established method and therefore for the purpose of comparing the model to the test results (Figure 11), the proposed model is terminated such that the ultimate displacement matches that obtained from the experimental tests.

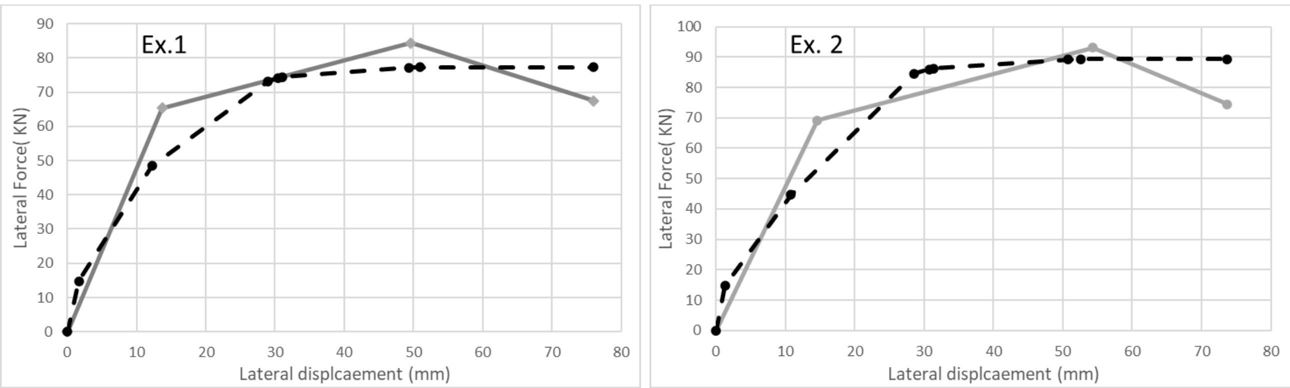

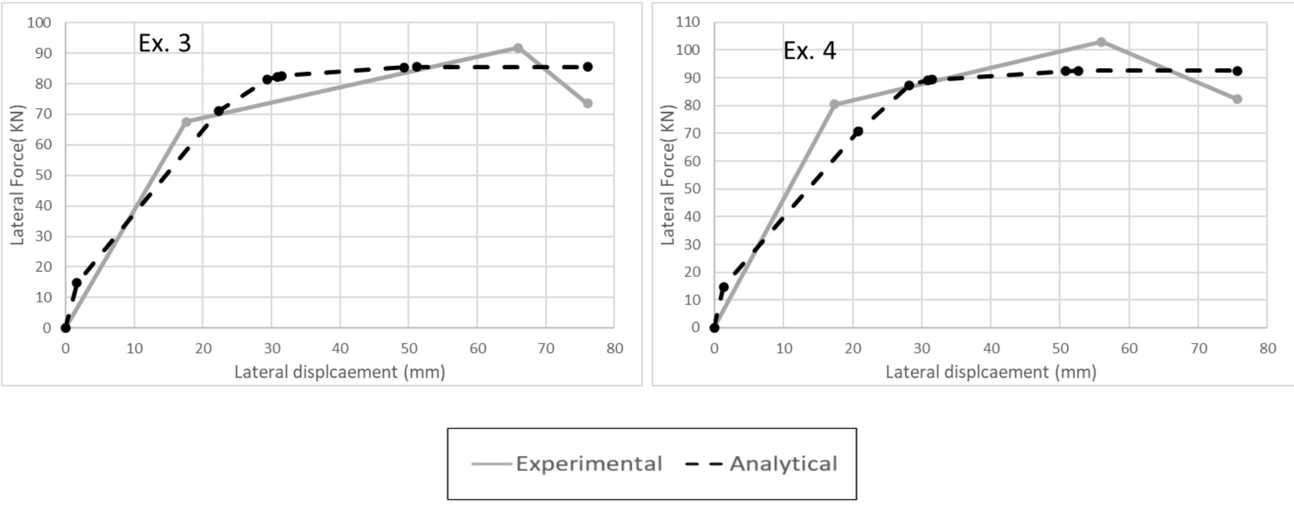

Figure 11: The curves from analytical and experimental results

Table 6: Comparison between the experimental results from [21] and analytical methods

Comparison	Ex.1	Ex.2	Ex.3	Ex.4
$F_{max,ex}/F_{max,an}$	1.08	1.02	1.06	1.09
K_{ex}/K_{an}	1.04	1.05	0.99	1.12

5. Conclusion

Elastic analytical methods for multi-panel CLT shearwalls, including the bi-axial contribution of the angle brackets and hold-downs, have been developed using the method of minimum potential energy. Expressions are developed in the elastic region to establish the coupled-panel and single-wall kinematic behaviours of the shearwall, and kinematic regions, depicting areas where different kinematic modes govern the behaviour of the wall are investigated. The inelastic expressions are provided for the coupled-panel behaviour as the initial elastic and ultimate inelastic behaviour.

The conclusions that can be drawn from the current study are:

- As expected, when the bi-axial effect of the angle brackets is considered in the analysis, especially for relatively stiff angle brackets in vertical direction and higher number of angle brackets, more panels are likely to maintain contact with the ground, resulting in less displacements and rotations. It was also observed that as the number of panels increases, the SW region becomes smaller for all values of angle bracket stiffness, since more connectors are involved in resisting the vertical uplift load.

- Results from the sensitivity analyses showed that the biaxial contribution of the angle brackets may be neglected if relatively flexible angle brackets are used ($\emptyset < 0.125$), while ensuring CP behaviour. In those cases, a maximum difference of 17% or less is obtained. When the SW behaviour is attained, considering the bi-axial effect of angle brackets is required, since neglecting such effect would lead to errors of at least 20%.
- The proposed methodologies for the elastic and inelastic models are verified using a numerical model and validated with results from published experimental tests. The results obtained from inelastic analysis show that the analytical solution matches that obtained from the numerical model almost perfectly. Reasonable match is observed in terms of general shape of the results' curves and maximum lateral capacity of the shearwalls when the proposed model is compared to the test results.

Future efforts by the authors aims at validating the proposed methodologies and expressions through extensive experimental testing on multi-panel CLT Shearwalls.

References

[1] CSA O86:19: Engineering design in wood, Mississauga: CSA Group, 2019.

[2] CEN, European Standard EN 1995: Eurocode 5: Design of timber structures, Brussels, Belgium: European Committee for Standardization, 2004.

[3] A. Ceccotti, C. Sandhass, M. Okabe, M. Yasumura, C. Minowa and N. Kawai, “SOFIE project– 3D shaking table test on a seven-storey full-scale cross-laminated building,” *Earthquake Engineering and Structural Dynamic,* vol. 42, no. 13, 2013, http://dx.doi.org/10.1002/eqe.2309.

[4] V. Histovski, V. Mircevska, B. Dujic and M. Garevski, “Comparative dynamic investigation of cross-laminated wooden panel systems: Shaking-table tests and analysis,” *Advanced in Structural Engineering,* vol. 21, no. 10, pp. 1421-1436, 2017, http://dx.doi.org/10.1177/1369433217749766.

[5] M. Izzi, D. Casagrande, S. Bezzi, D. Pasca, M. Follesa and R. Tomasi, “Seismic behaviour of Cross-laminated timber structrures: A state-of-the-art review,” *Engineering Structures,* vol. 170, pp. 42-52, 2018, https://doi.org/10.1016/j.engstruct.2018.05.060.

[6] G. Flatscher, K. Bratulic and G. Schickhofer, “Experimental tests on cross-laminated timber joints and walls,” *Proceedings of the Institution of Civil Engineers - Structures and Buildings,* vol. 168, no. 11, pp. 868-877, 2015, http://dx.doi.org/10.1680/stbu.13.00085.

[7] M. Popovski and I. Gavric, “Performance of a 2-storey CLT house subjected to lateral load,” *Journal of Structural Engineering,* vol. 142, no. 4, 2016, https://doi.org/10.1061/(ASCE)ST.1943-541X.0001315.

[8] M. Yasumura, K. Kobayashi, M. Okabe, T. Miyake and K. Matsumoto, “Full-scale tests and numerical analysis of low-rise CLT structures under lateral loading,” *Journal of*

Structural Engineering, vol. 142, no. 4, 2016, http://dx.doi.org/10.1061/(ASCE)ST.1943-541X.0001348.

[9] G. Rinaldin and M. Fragiacomo, “Non-linear simulation of shaking-table tests on 3- and 7-storey X-Lam timber buildings,” *Engineering Structures,* vol. 113, pp. 133-148, 2016, http://dx.doi.org/10.1016/j.engstruct.2016.01.055.

[10] Y. Shen, J. Schneider, S. Tesfamariam, S. F. Stiemer and Z. Mu, “Hysteresis behavior of bracket connection in cross-laminated-timber shear walls,” *Construction and Building Materials,* vol. 48, pp. 989-991, 2013, http://dx.doi.org/10.1016/j.conbuildmat.2013.07.050.

[11] I. Gavric, M. Fragiacomo and A. Ceccotti, “Cyclic behaviour of typical metal connectors for cross-laminated (CLT) structures,” *Materials and Structures,* vol. 48, p. 1841–1857, 2015, https://doi.org/10.1617/s11527-014-0278-7.

[12] J. Schneider, Y. Shen, S. Stiemer and S. Tesfamariam, “Assessment and comparison of experimental and numerical model studies of cross-laminated timber mechanical connections under cyclic loading,” *Construction and Building Materials,* vol. 77, pp. 192-212, 2015, http://dx.doi.org/10.1016/j.conbuildmat.2014.12.029.

[13] L. Pozza, A. Saetta, M. Savoia and D. Talledo, “Coupled axial-shear numerical model for CLT connections,” *Construction and Building Materials,* vol. 150, pp. 568-582, 2017, http://dx.doi.org/10.1016/j.conbuildmat.2017.05.141.

[14] L. Pozza, A. Saetta, M. Savoia and D. Talledo, “Angle bracket connections for CLT structures: Experimental characterization and numerical modelling,” *Construction and Building Materials,* vol. 191, pp. 95-113, 2018, https://doi.org/10.1016/j.conbuildmat.2018.09.112.

[15] L. Pozza, B. Ferracuti, M. Massari and M. Savoia, “Axial – Shear interaction on CLT hold-down connections – Experimental investigation,” *Engineering Structures,* vol. 160, pp. 95-110, 2018, https://doi.org/10.1016/j.engstruct.2018.01.021.

[16] J. Liu and F. Lam, “Experimental test of coupling effect on CLT angle bracket connections,” *Engineering Structures,* vol. 171, pp. 862-873, 2018, https://doi.org/10.1016/j.engstruct.2018.05.013.

[17] J. Liu and F. Lam, “Experimental test of coupling effect on CLT hold-down connections,” *Engineering Structures,* vol. 178, pp. 586-602, 2019, https://doi.org/10.1016/j.engstruct.2018.10.063.

[18] J. Liu, F. Lam, R. O. Foschi and M. Li, “Modeling the Coupling Effect of CLT Connections under Biaxial Loading,” *Journal of Structural Engineering,* vol. 146, no. 4, 2020, https://doi.org/10.1061/(ASCE)ST.1943-541X.0002589.

[19] G. D'Arenzo, G. Rinaldin, M. Fossetti and M. Fragiacomo, “An innovative shear-tension angle bracket for Cross-Laminated Timber structures: Experimental tests and numerical modelling,” *Engineering Structures,* vol. 197, 2019,

https://doi.org/10.1016/j.engstruct.2019.109434.

[20] I. Lukacs, A. Björnfot and R. Tomasi, “Strength and stiffness of cross-laminated timber (CLT) shear walls: State-oft-the-art of analytical approaches,” *Engineering Structures,* vol. 178, pp. 136-147, 2019, https://doi.org/10.1016/j.engstruct.2018.05.126.

[21] I. Gavric, M. Fragiacomo and A. Ceccotti, “Cyclic Behaviour of CLT wall systems: Experimental tests and analytical prediction models,” *Journal of Structural Engineering,* vol. 141, no. 11, 2015, https://doi.org/10.1061/(ASCE)ST.1943-541X.0001246.

[22] G. Flatscher and G. Schickhofer, “Displacement-based determination of laterally loaded Cross Laminated Timber (CLT) wall systems,” In INTER - International Network on Timber Engineering Research [INTER/49-12-1]., 2016.

[23] G. Tamagnone, G. Rinaldin and M. Fragiacomo, “A novel method for non-linear design of CLT wall systems,” *Engineering Structures,* vol. 167, pp. 760-771, 2018, https://doi.org/10.1016/j.engstruct.2017.09.010.

[24] D. Casagrande, D. Ghasan, L. Mauro and A. Polastri, “Analytical Approach to Establishing the Elastic Behavior of Multipanel CLT Shear Walls Subjected to Lateral Loads,” *Journal of Structural Engineering,* vol. 144, no. 2, 2018, https://doi.org/10.1061/(ASCE)ST.1943-541X.0001948.

[25] V. Nolet, D. Casagrande and D. Ghasan, “Multipanel CLT shearwalls: an analytical methodology to predict the elasticplastic,” *Engineering Structures,* vol. 179, pp. 640-654,

2019, https://doi.org/10.1016/j.engstruct.2018.11.017.

[26] ETA-06/0106, “European Technical Assessment-Three-dimensional nailing plate (timber-to-timber/timber-to-concrete angle bracket),” European Organisation for Technical Approvals, Nordhavn, Denmark, 2016.

[27] M. Izzi, A. Polastri and M. Fragiacomo, “Modelling the mechanical behaviour of typical wall-to-floor connection systems for Cross-Laminated Timber structures,” *Engineering Structures,* vol. 162, no. 2, pp. 70-82, 2018, https://doi.org/10.1016/j.engstruct.2018.02.045.

[28] D. Casagrande, S. Rossi, R. Tomasi and G. Mischi, “A predictive analytical model for the elasto-plastic behaviour of a light timber-frame shear-wall,” *Construction and Building Materials,* vol. 102, p. 1113–1126, 2016, https://doi.org/10.1016/j.conbuildmat.2015.06.025.

[29] R. Brandner, P. Dietsch, J. Dröscher, M. Schulte-Wrede, H. Kreuzinger and M. Sieder, “Cross laminated timber (CLT) diaphragms under shear: Test configuration, properties and design,” *Construction and Building Materials,* vol. 147, pp. 312-327, 2017, https://doi.org/10.1016/j.conbuildmat.2017.04.153.

[30] CSI, “SAP2000 Integrated Software for Structural Analysis and Design,” Computers and Structures Inc., Berkeley, California.

[31] ASTM E2126, "Standard test methods for cyclic (reversed) load test for shear resistance of vertical elements of the lateral force resisting systems for buildings", West Conshohocken, PA: American Society for Testing and Materials (ASTM), 2011, DOI: 10.1520/E2126-11.